Air-sea interactions and water mass structure of the East China Sea and Yellow Sea

Kuninaka, Akira

Monterey, California. Naval Postgraduate School

NAVAL POSTGRADUATE SCHOOL
Monterey, California

THESIS

**AIR-SEA INTERACTIONS
AND WATER MASS STRUCTURE
OF THE EAST CHINA SEA AND YELLOW SEA**

by

Akira Kuninaka

March 1998

Thesis Advisors: Peter C. Chu
Robert H. Bourke

Approved for public release; distribution is unlimited.

REPORT DOCUMENTATION PAGE

Form Approved OMB No. 0704-0188

1. AGENCY USE ONLY *(Leave blank)*	2. REPORT DATE March 1998	3. REPORT TYPE AND DATES COVERED Master's Thesis

4. TITLE AND SUBTITLE
AIR-SEA INTERACTIONS AND WATER MASS STRUCTURE OF THE EAST CHINA SEA AND YELLOW SEA

5. FUNDING NUMBERS

6. AUTHOR(S) Akira Kuninaka

7. PERFORMING ORGANIZATION NAME(S) AND ADDRESS(ES)
Naval Postgraduate School
Monterey CA 93943-5000

8. PERFORMING ORGANIZATION REPORT NUMBER

9. SPONSORING/MONITORING AGENCY NAME(S) AND ADDRESS(ES)

10. SPONSORING/MONITORING AGENCY REPORT NUMBER

11. SUPPLEMENTARY NOTES The views expressed in this thesis are those of the author and do not reflect the official policy or position of the Department of Defense or the U.S. Government.

12a. DISTRIBUTION/AVAILABILITY STATEMENT
Approved for public release; distribution is unlimited.

12b. DISTRIBUTION CODE

13. ABSTRACT *(maximum 200 words)*

The climatological water mass features, the seasonal variabilities of the thermohaline structure, and the linkage between fluxes (momentum, heat, and moisture) of the East China and Yellow Seas have been investigated. The long term mean surface heat balance corresponds to a heat gain of 15 W m^{-2} in the Yellow Sea shelf (YS), a heat loss of around 30 W m^{-2} in the East China Sea shelf (ECS) and Cheju bifurcation zone (CB), and around 65 W m^{-2} in the Taiwan Warm Current region (TWC) and Kuroshio Current region (KC). The surface fresh water balance, i.e., evaporation minus precipitation, ranges from -1.8 to -4.0 cm/month for the five subareas. The four seasons for the study area are divided based on the relative heat storage, which do not follow the usual atmospheric seasons. The entire water column of the ECS, YS and CB undergoes a seasonal thermal cycle with maximum values of temperature during summer and maximum mixed layer depths during winter. Only the surface waters of TWC and KC exhibit a seasonal thermal cycle. Two patterns exist in the surface salinity and Yangtze River run-off, out of phase in the East China Sea and in phase in the Yellow Sea.

14. SUBJECT TERMS Water mass features, thermohaline structures, seasonal cycle			15. NUMBER OF PAGES 75 16. PRICE CODE
17. SECURITY CLASSIFICATION OF REPORT Unclassified	18. SECURITY CLASSIFICATION OF THIS PAGE Unclassified	19. SECURITY CLASSIFICATION OF ABSTRACT Unclassified	20. LIMITATION OF ABSTRACT UL

NSN 7540-01-280-5500

Standard Form 298 (Rev. 2-89)
Prescribed by ANSI Std. 239-18 298-102

Approved for public release; distribution is unlimited.

AIR-SEA INTERACTIONS AND WATER MASS STRUCTURE OF THE EAST CHINA SEA AND YELLOW SEA

Akira Kuninaka
Lieutenant Commander, Japan Maritime Self Defense Force
B.S., University of The Ryukyus, 1984

Submitted in partial fulfillment
of the requirements for the degree of

MASTER OF SCIENCE IN PHYSICAL OCEANOGRAPHY

from the

NAVAL POSTGRADUATE SCHOOL
March 1998

ABSTRACT

The climatological water mass features, the seasonal variabilities of the thermohaline structure, and the linkage between fluxes (momentum, heat, and moisture) of the East China and Yellow Seas have been investigated. The long term mean surface heat balance corresponds to a heat gain of 15 W m^{-2} in the Yellow Sea shelf (YS), a heat loss of around 30 W m^{-2} in the East China Sea shelf (ECS) and Cheju bifurcation zone (CB), and around 65 W m^{-2} in the Taiwan Warm Current region (TWC) and Kuroshio Current region (KC). The surface fresh water balance, i.e., evaporation minus precipitation, ranges from -1.8 to -4.0 cm/month for the five subareas. The four seasons for the study area are divided based on the relative heat storage, which do not follow the usual atmospheric seasons. The entire water column of the ECS, YS and CB undergoes a seasonal thermal cycle with maximum values of temperature during summer and maximum mixed layer depths during winter. Only the surface waters of TWC and KC exhibit a seasonal thermal cycle. Two patterns exist in the surface salinity and Yangtze River run-off, out of phase in the East China Sea and in phase in the Yellow Sea.

TABLE OF CONTENTS

I. INTRODUCTION 1

II. ECS/YS OCEANOGRAPHY AND SUBDIVISION 5

A. CURRENT SYSTEM 5

B. WATER MASSES 6

C. SUBDIVISION 7

III. SEASONAL VARIATION OF THE ATMOSPHERIC SURFACE FORCING . . 11

A. GENERAL DESCRIPTION 11

B. SURFACE CLIMATOLOGY 13

C. SURFACE FLUXES 15

1. Net Heat Flux 15

2. Fresh water flux 26

3. Surface Buoyancy Flux 26

IV. THE HYDROGRAPHIC DATA SET 31

V. SEASONAL VARIATION OF WATER MASS STRUCTURE 35

A. RELATIVE HEAT STORAGE 35

B. TEMPERATURE AND SALINITY 37

VI. INTERANNUAL VARIATION OF THERMOHALINE STRUCTURE 47

VII. CONCLUSIONS 59

LIST OF REFERENCES 61

INITIAL DISTRIBUTION 63

ACKNOWLEDGMENTS

The author would like to acknowledge the unfailing support of C. W. Fan and Yuchun Chen for their programming assistance. Special thanks to Dr. Peter C. Chu and Dr. Robert H. Bourke for their guidance and patience. This work was funded by the Naval Oceanographic Office, the Office of Naval Research NOMP Program, and the Naval Postgraduate School.

I. INTRODUCTION

The combined East China Sea and Yellow Sea (ECS/YS) covers roughly 1,250,000 km^2 and is one of the most developed continental shelf areas in the world (Yanagi and Takahashi, 1993). While the Yellow Sea (YS) covers a relatively large area, it is quite shallow reaching a maximum depth of about 140 m (Figure 1). The water depth over most of the area is less than 50 m. The deepest water is confined to a north-south oriented trench which runs from the northern boundary south to the 100 m isobath where it fans out onto the continental shelf break. The bathymetric gradients are very small. Such a broad and shallow continental shelf sea suggests that the water column will be readily affected by seasonally varying atmospheric conditions such as heating, cooling, and wind stress. Therefore, the seasonal variation of the water masses is remarkably large. Another feature of the depth distribution is the east/west asymmetry. Extensive shoals (< 20 m) are located in the western Yellow Sea along the Chinese coast but are not generally found off the South Korea coastal regions. Also, the 50 m isobath is located more than 100 km from the Chinese coast, but only about 50 km from the South Korea coast. This asymmetry in bottom depth is important in controlling the mixed layer depth (Chu et al., 1997b).

The East China Sea (ECS) is located south of the YS to the north of Taiwan (Figure 1). The ECS is usually defined as reaching from the northern end of Taiwan Strait to the southern end of Kyusyu where it adjoins the YS along a line from Kyusyu to Shanghai (the mouth of the Yangtze River). With the exception of the Okinawa Trough west of the Ryukyu Islands, which reaches 2,700 m depth, the ECS is part of the continental shelf. The

hydrographic character of the water masses in the ECS/YS system depends on the bathymetry, the Kuroshio Current, the atmospheric forcing (monsoon winds, heat and moisture fluxes), and degree of mixing of fresh water originating from the Asian river runoff with the intrusion of Kuroshio waters (Tomczak and Godfrey, 1994).

To examine the seasonal variability of the water mass and circulation, we use the U.S. Navy's Master Oceanographic Observation Data Set (MOODS) to investigate the climatological water mass features and the seasonal and non-seasonal variabilities of the thermohaline structure, and use the Comprehensive Ocean-Atmosphere Data Set (COADS) from 1945 to December 1989 to investigate the linkage between the fluxes (momentum, heat, and moisture) across the air-ocean interface and the formation of the water mass features.

The structure of the rest of this paper is outlined as follows. In Section 2, we partition the ECS/YS into five subareas according the bottom topography and circulation pattern. In Section 3, we define the surface atmospheric conditions, air-ocean heat, fresh water, and momentum fluxes for the five sub-regions. In Section 4, we discuss the major features of the MOODS data set. In Section 5, we classify the seasons according to the heat storage and study the seasonal variation of the water masses for the five sub-regions. In Section 6, we investigate the interannual variation of the water mass structure.

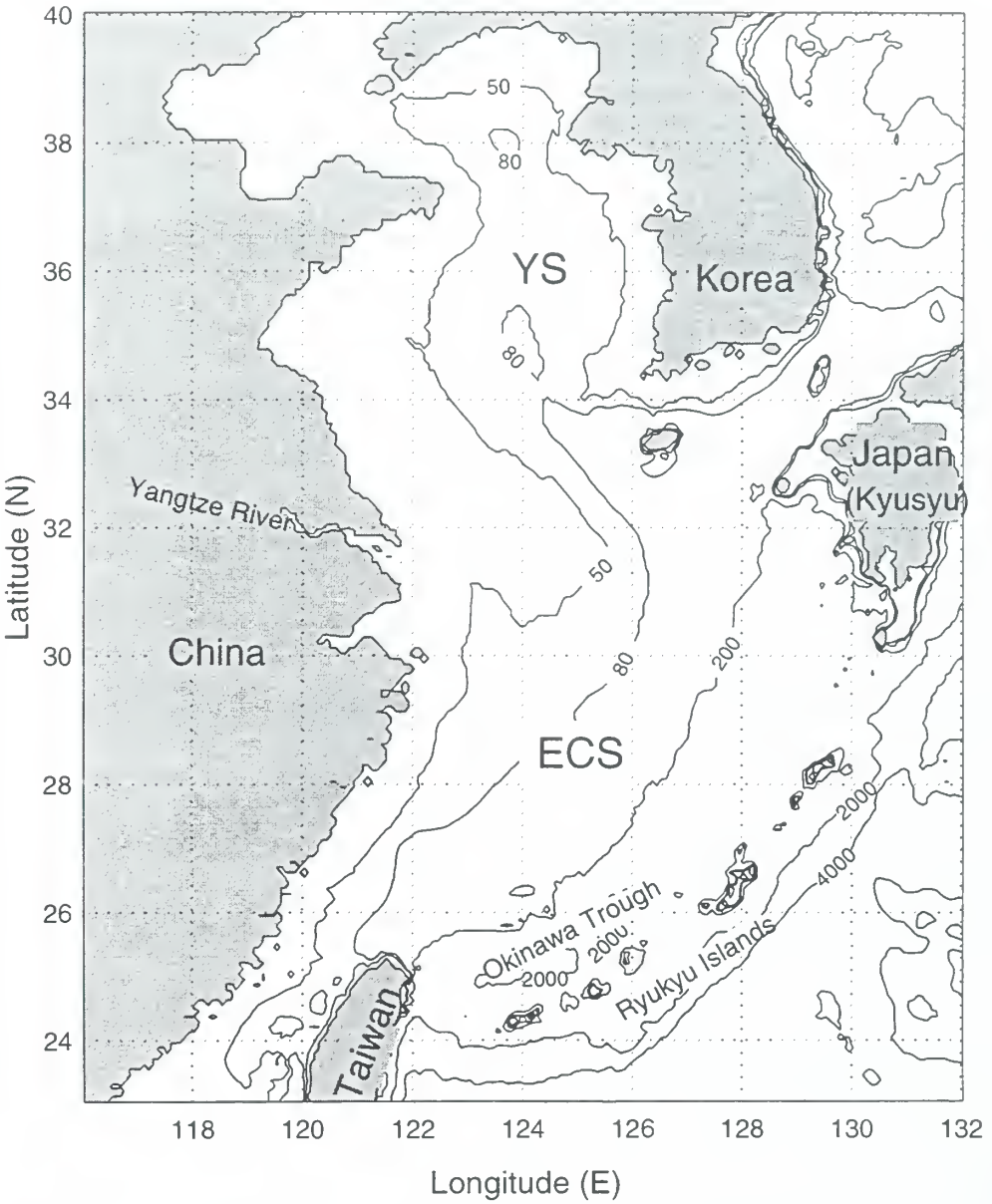

Figure 1. Topography and isobaths of the East China Sea and the Yellow Sea.

II. ECS/YS OCEANOGRAPHY AND SUBDIVISION

A. CURRENT SYSTEM

Niino and Emery (1961), Mao and Guan (1982), and Guan (1994) have constructed the general circulation pattern of the ECS/YS based on limited accessible scientific literature. Beardsley et al. (1985) provide a complete description of the ECS/YS general circulation which is outlined briefly below. Over the outer continental shelf, the Kuroshio Current (KC) flows northeastward and has a maximum transport in summer (Figure 2). Inshore of the Kuroshio, a warm, saline current called the Taiwan Warm Current (TWC) also flows northeastward, but unlike the Kuroshio which flows offshore to the south of Japan, the TWC flows into the Japan Sea through the Tsushima Strait between Korea and Japan. Some TWC water flows intermittently northward into the YS along the Korean coast (Tomczak and Godfrey, 1994). The semi-enclosed Gulf of Bohai and north YS is characterized by northward inflow of saline water along the Korean coast and outflow of less saline water along the coast of the Shangdong Peninsula. The magnitude of the fresh water discharge of Huanghe (the Yellow River) which drains into the Gulf of Bohai is smaller than that of Changjiang (the Yangtze River). In winter, some southward-flowing coastal water along the coast of Jiangsu continues southward along the coast of Zhejiang Province, and some Jiangsu coastal water flows offshore in a downwind, southeastward direction from a point just north of the mouth of Changjiang. Guan (1994) partitioned the ECS/YS general circulation into two sub-systems: the warm and saline current system of oceanic origin (Kuroshio and its branches and extensions) and the less saline coastal current system. The former moves northward while

the latter generally flows southward.

B. WATER MASSES

Earlier studies (e.g., Liu et al., 1992; Su and Weng, 1994, Chen et al., 1995) have shown that a complex water mass structure exists in the ECS/YS based on temperature and salinity features. The water in the shallow parts of the ECS/YS is affected greatly by the atmospheric and geographic conditions, and therefore it does not have the homogeneity as in the open ocean. Su and Weng (1994) proposed a concept of modified water masses for a water body which holds similar physical and chemical characteristics and occupies a certain space.

Based on temperature data observed in 1978-1980, Su et al. (1983) identified the following water masses using a successive clustering method on temperature observations: Kuroshio Surface Water (KSW), East China Sea Mixed Water (ECSMW), East China Sea Deep Water (ECSDW), Yellow Sea and East China Sea Mixed Water (YESMW), Yellow Sea Mixed Water (YSMW), Yellow Sea Bottom Cold Water (YSCW), Yellow Sea Near-shore Water (YSNW), and Continental Shelf Diluted Water (CSDW) (Figure 3).

Since salinity is a more conserved quantity in the ECS/YS than temperature (Su and Weng, 1994), the water masses are classified into three systems based on their salinity features: (i) the ECS water system (or the open water system), including KSW, ECSMW, ECSDW, and YESMW (in May only) and originated from the Kuroshio Water Mass, (ii) the YS water system (or the local water system), including YSMW, YSCW, YESMW, and (iii) coastal water system, including CSDW and YSNW.

Since the ECS water system is an open water system, horizontal advection especially

meandering of the Kuroshio Current, should be an important factor in its variability. In contrast, the YS water system is a local system. The local atmospheric forcing should be responsible for its variability. In fact, the central region of the YS stands out due to its cold bottom water, that is YSCW. During summer, strong surface warming generates the sharpest thermocline on the top of the YSCW in the region. During winter, this water mass provides a significant buffer preventing central YS water temperatures from reaching the near-freezing temperatures that the near-shore regions experience (Chu et al., 1997b).

C. SUBDIVISION

After examining the major current systems and considering the local bathymetry and water mass properties, we have divided the ECS/YS into five regions (Figure 4): (1) the ECS shelf with the eastern boundary at the 80 m bathymetry contour line and the northern boundary at 32° N, representing the coastal current system; (2) the YS shelf with the northern boundary at 38°30' N, the southern boundary at 32° N, the western boundary at 122° E in the mouth of Gulf of Bohai and the Chinese coast, and the eastern boundary at the Korean coast and 80 m depth contour line, representing the YS gyre system; (3) the Cheju bifurcation (CB) area with the northern and western boundaries at 80 m contour, the eastern boundary at 127°15' E, and the southern boundary at 32° N, representing the TWC branching into Tsushima Current and Yellow Sea Warm Current (Figure 2); (4) the Taiwan Warm Current area bounded by the 80 m and 200 m bathymetric contours, and 32° N latitude, representing the TWC system; and (5) the Kuroshio area bounded by the 200 m and 4000 m contours, and 32° N latitude, representing the KC system.

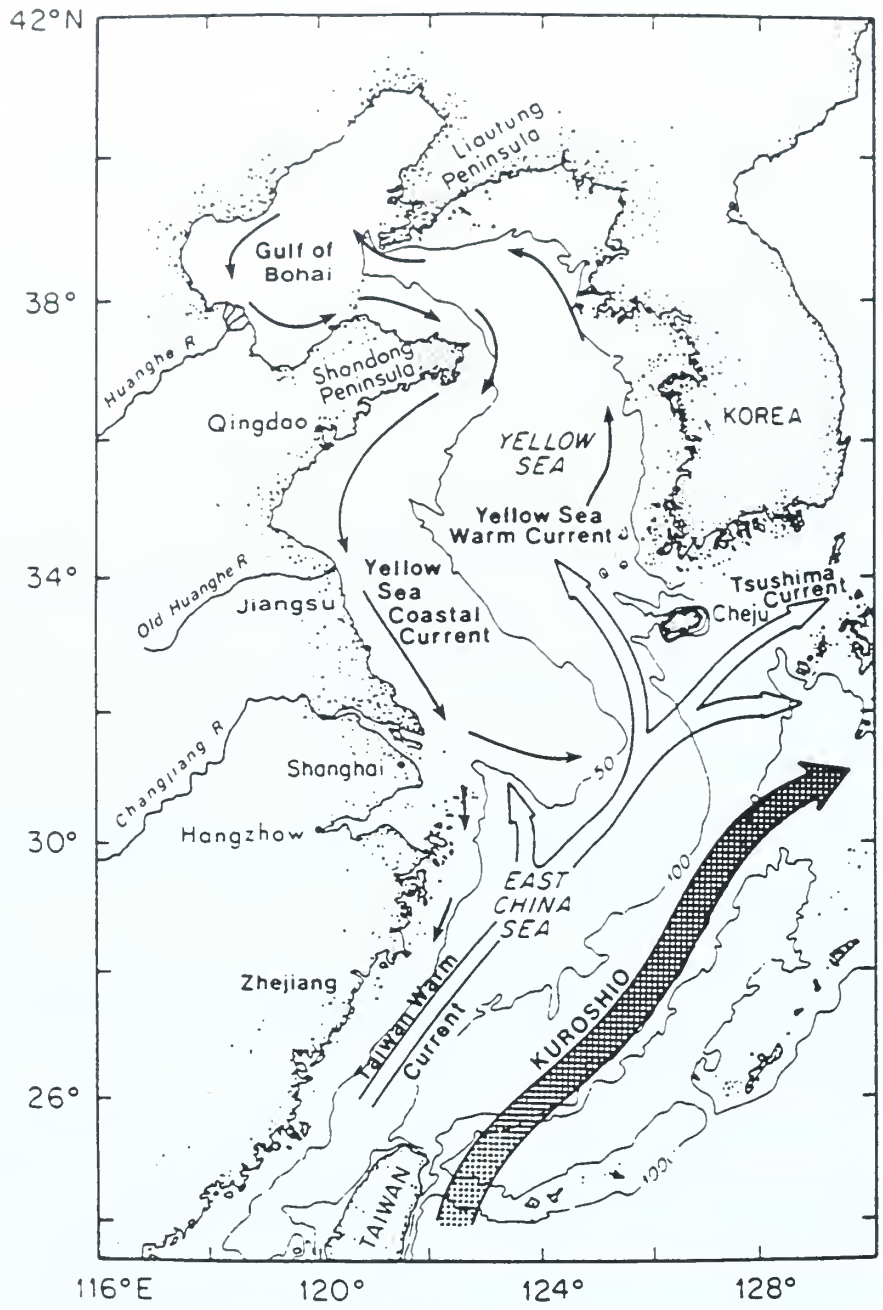

Figure 2. General circulation in ECS/YS [from *Beardsley et al.*, 1985].

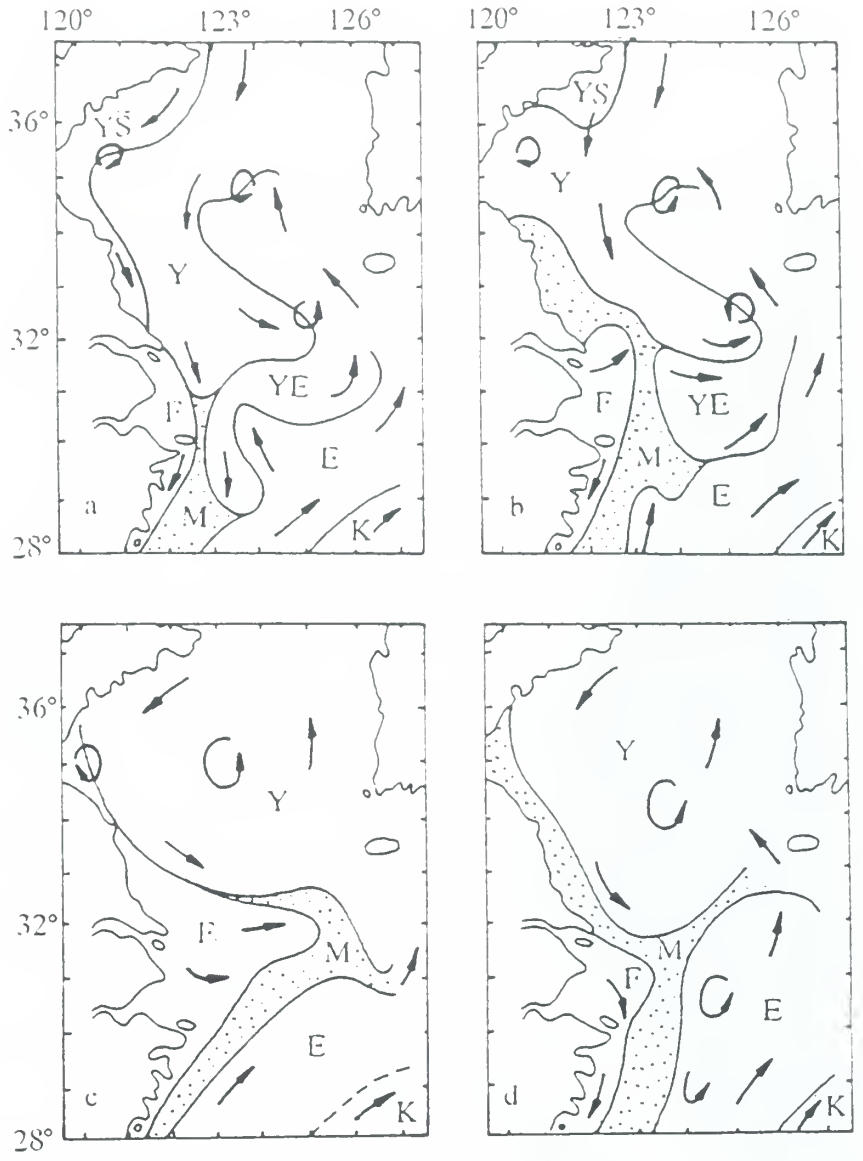

Figure 3. Water mass distribution and circulation patterns at the ECS/YS surface for (a) February, (b) May, (c) August, and (d) November. Here, Y-Yellow Sea Mixed Water, YS-Yellow Sea Nearshore Water, YE-Yellow Sea and East China Sea Mixed Water, M-Fully Mixed Water, K-Kuroshio Water, F-Continental Coastal Diluted Water [from *Su and Weng*, 1994].

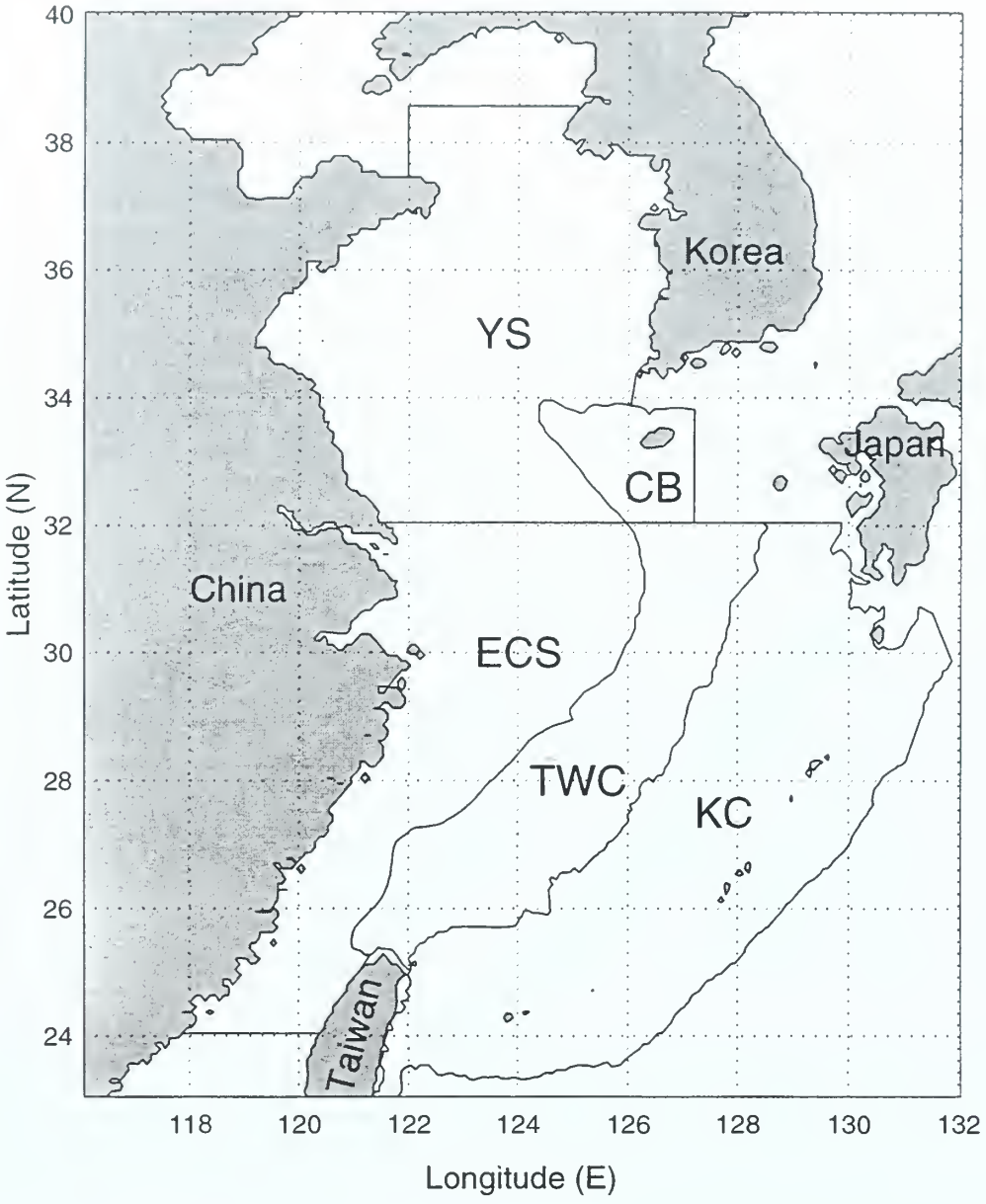

Figure 4. Subdivisions of ECS/YS.

III. SEASONAL VARIATION OF THE ATMOSPHERIC SURFACE FORCING

A. GENERAL DESCRIPTION

The Asian monsoon strongly affects the thermal structure of the ECS/YS. During the winter monsoon season, a very cold northwest wind blows over the ECS/YS as a result of the Siberian High Pressure System. The Jet Stream is positioned to the south of the YS and the Polar Front to the north of the Philippines (Figure 5(a)). By late April the Polar Front has moved northward toward Korea with warm, moist air following behind. Numerous frontally-generated events occur making late April and May highly variable in terms of wind speeds and cloud amount. During this period storms originating in Mongolia may cause strong, warm westerlies carrying yellow desert sand (termed the "Yellow Wind"). By late May and early June the summer surface atmospheric low pressure system begins to form over Asia. Initially this low pressure system is centered north of the Yellow Sea producing westerly winds. In late June this low begins to migrate to the west setting up the southwest monsoon that dominates the summer months. The winds remain variable through June until strengthening of the Manchurian Low pressure system occurs. The Jet Stream migrates just south of Korea, and the Polar Front is just south of Kyusyu and Shikoku. Despite the very active weather systems, the mean surface wind speed over the central Yellow Sea in summer is between 3 and 4 m/s, which is weaker than in winter (Figure 5(b)) (Chu et al., 1997a). June also marks, historically, a jump in precipitation associated with warm, moist air south of the Polar Front (Watts, 1969). Occasionally the Okhotsk High blocks the northerly progression of the Polar Front. By July, however, high pressure (the Bonin High) to the south and the

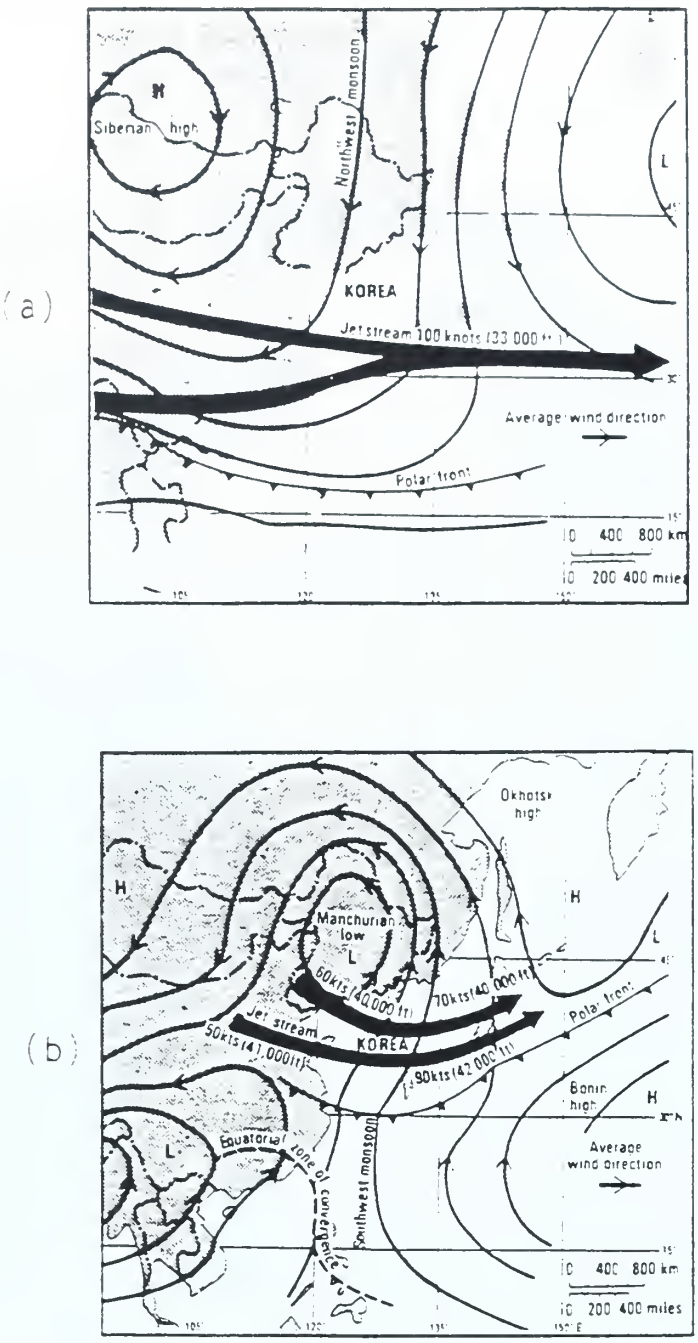

Figure 5. Mean locations of pressure systems and winds for (a) February and (b) June [from *Langhill*, 1976].

low pressure over Manchuria produce southerly winds carrying warm, moist air over the ECS/YS. The summer monthly mean surface air temperature (SAT) is usually 1.5°-2°C warmer than the mean sea surface temperature (SST) (Van Loon, 1984). The warmer air causes a downward heat flux at the air-ocean interface. This heat flux plus the strong downward net radiation stabilizes the upper layer of the water and causes the surface mixed layer to shoal, creating a multilayered structure. Below the thermocline in the YS, there is a cold water mass, commonly referred to as Yellow Sea Bottom Cold Water (YSCW), that remains unchanged and nearly motionless throughout the summer (Li and Yuan, 1992). October is the beginning of the transition back to winter conditions. The southerly winds weaken letting the sea surface slope reestablish the winter pattern. The SST steadily decreases from October to January (Chu et al., 1997b).

B. SURFACE CLIMATOLOGY

Here, we present a climatological description of the atmospheric conditions over the ECS/YS and their effect in terms of heat exchange and storage. One of the datasets used was the objectively analyzed fields of surface marine climatology and anomalies of fluxes of heat, momentum, and fresh water. The fields are derived from individual observations in the Comprehensive Ocean-Atmosphere Data Set (COADS) from 1945 to 1989 and are analyzed on a 1° by 1° grid. The climatological monthly mean values of windspeed, temperature and relative humidity are shown in Figures 6-8 for the months of February, May, August, and November, which may be regarded as representative patterns for each season.

The main characteristic of the COADS wind data (Figure 6) is the seasonal variation of the monsoon winds. In winter, strong north to northwest winds prevail in the northern

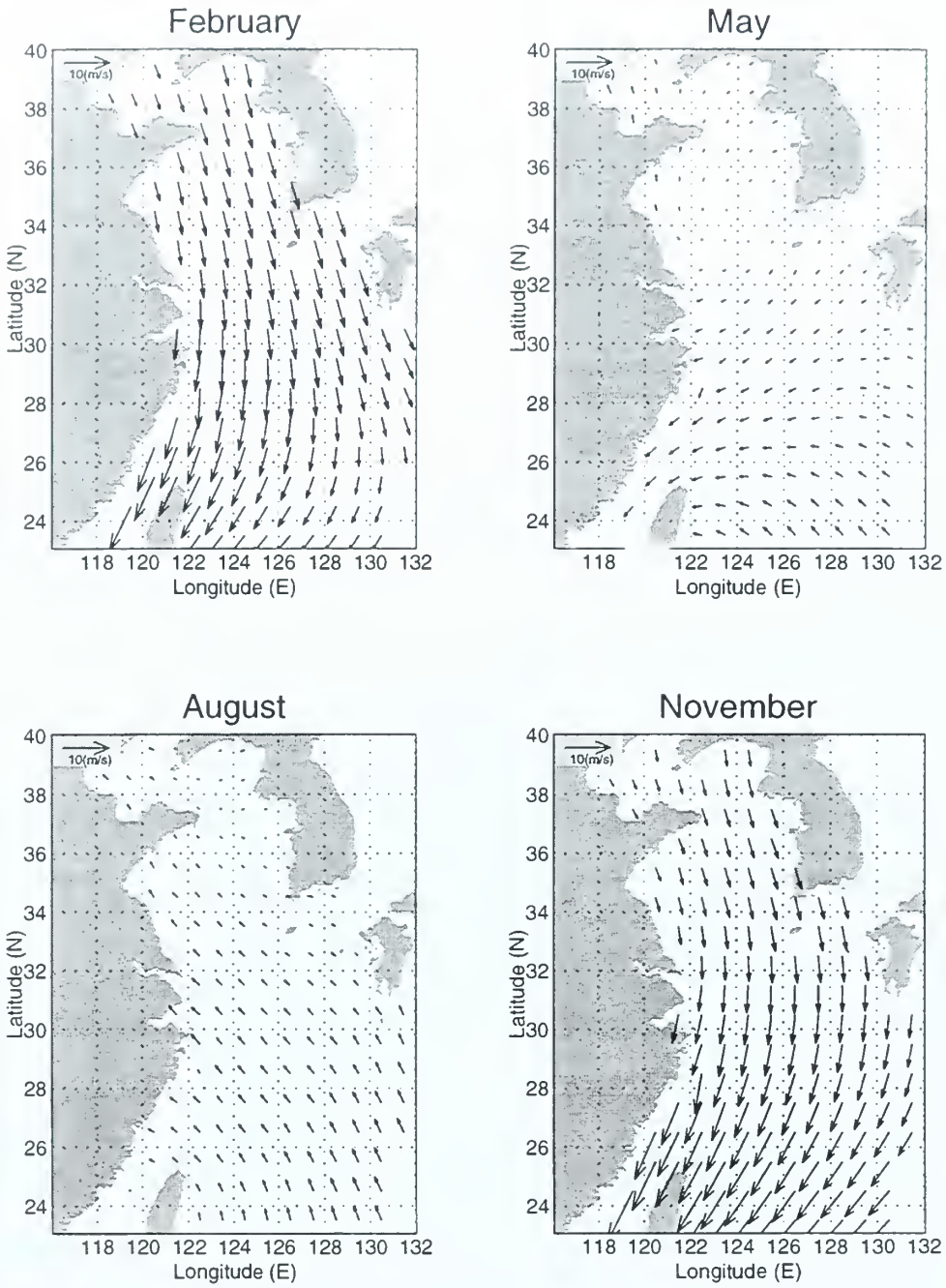

Figure 6. Average wind speed (m/s) for February, May, August and November from COADS.

ECS/YS and north to northeast winds prevail in the southern ECS/YS. In summer, weak southeast winds prevail. May is the summer monsoon transition period. The surface winds over the YS are very weak (mean monthly wind speed less than 3 m/s) both in summer and during the summer monsoon transition period.

The SAT exhibits seasonal fluctuations of about 22°C in the YS and about 10°C in the ECS, averaging about 17°C over the entire domain (Figure 7). A nearly latitudinal gradient prevails in all seasons with the maximum south-to-north mean SAT difference of 18°C in February and the minimum SAT difference of 3° C in August. The SAT is uniformly warm (mean SAT around 28°C) in the ECS during summer (August).

The surface relative humidity (Figure 8) is generally higher in the summer season, mainly as a consequence of the southeast summer monsoon bringing moist air from tropics. The summer field is relatively homogeneous (83%) in the ECS, whereas a significant latitudinal gradient exists during the rest of the seasons. A relative humidity minimum (maximum) is present in all seasons near Kyusyu Island (Chinese coast), which may lead to maximum (minimum) evaporation there.

C. SURFACE FLUXES

1. Net Heat Flux

The net surface heat flux is computed by

$$Q_{net} = R_S - (R_L + Q_S + Q_L)$$

where R_S is the net downward shortwave radiation, R_L the net upward longwave radiation, Q_S the sensible heat flux, and Q_L the latent heat flux. Positive values of Q_{net} indicate a heat

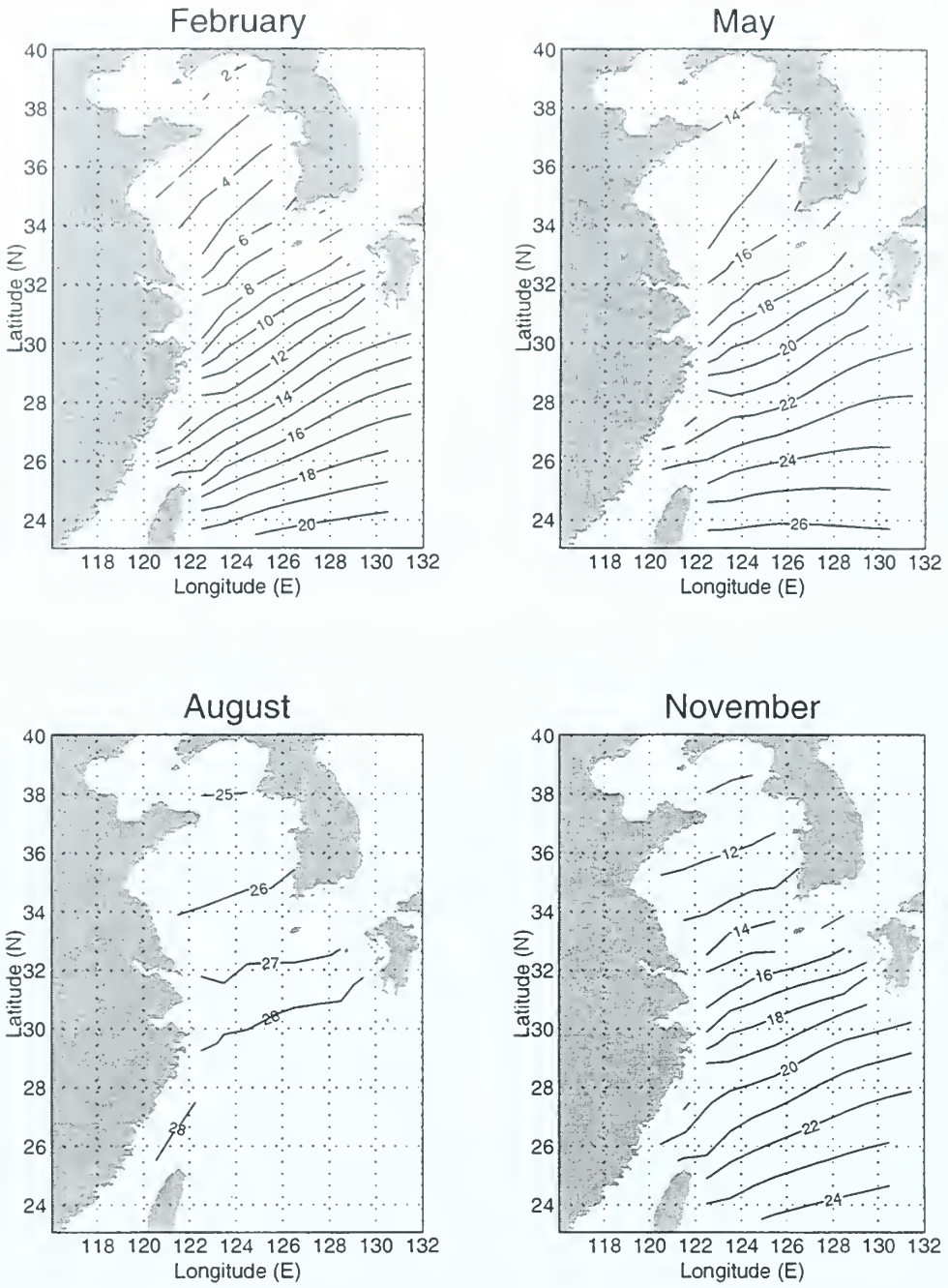

Figure 7. Average air temperature (°C) for February, May, August and November from COADS.

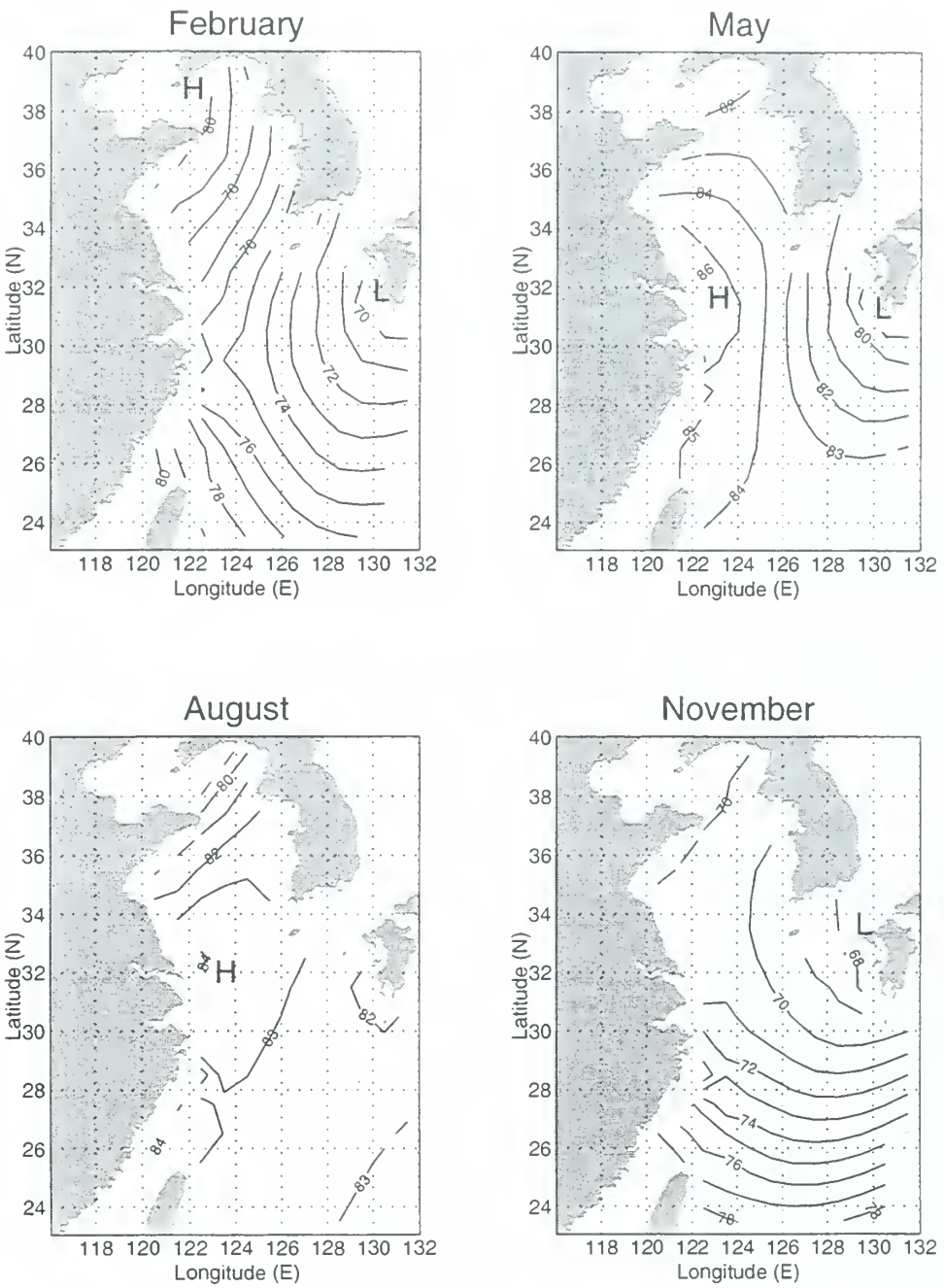

Figure 8. Average relative humidity (%) for February, May, August and November from COADS.

gain by the ocean at the surface. The COADS-derived heat flux (Figure 9) in summer is relatively homogeneous (120-160 W m^{-2}) over the whole ECS/YS. A significant horizontal gradient, with a minimum centered near Kyusyu Island, exists throughout the rest of the seasons. The ocean surface near Kyusyu Island (belonging to the KC and TWC sub-regions) exhibits a maximum heat loss of 280 W m^{-2} in the cold seasons (November, February), and also demonstrates a minimum heat gain of 80 W m^{-2} in spring. This long term net surface heat loss will be compensated by the advection of warm tropical waters by the KC and the TWC. There is an increase of net surface heat flux toward the Chinese coast in all seasons, which might be caused by less evaporation there.

The climatological monthly surface flux components for the five sub-areas are illustrated in Table 1 to Table 5. We see that latent heat and longwave radiation fluxes dominate the balance together with the solar radiation. The annual mean heat budget is positive in the YS region (15 W m^{-2}) and negative elsewhere: around -28 ~-32 W m^{-2} in the ECS and CB regions, and -65 W m^{-2} in the KC and TWC regions. A low annual mean latent heat flux in the YS region causes the positive annual heat budget. The sensible heat flux is nearly zero in summer, which implies a SST close to the SAT. The ratio between sensible and latent heat fluxes (defined as the Bowen ratio) is listed in the seventh column of these tables. The Bowen ratio has the following features: (a) values less than one for all months in all five sub-areas, indicating the latent heat flux is larger than the sensible heat flux, (b) a seasonal variation with relatively large values (0.33-0.67) in winter and near zero values in summer, and (c) larger annual variation in the shallow water regions (YS, CB) than in the relatively deep water regions (KC and TWC).

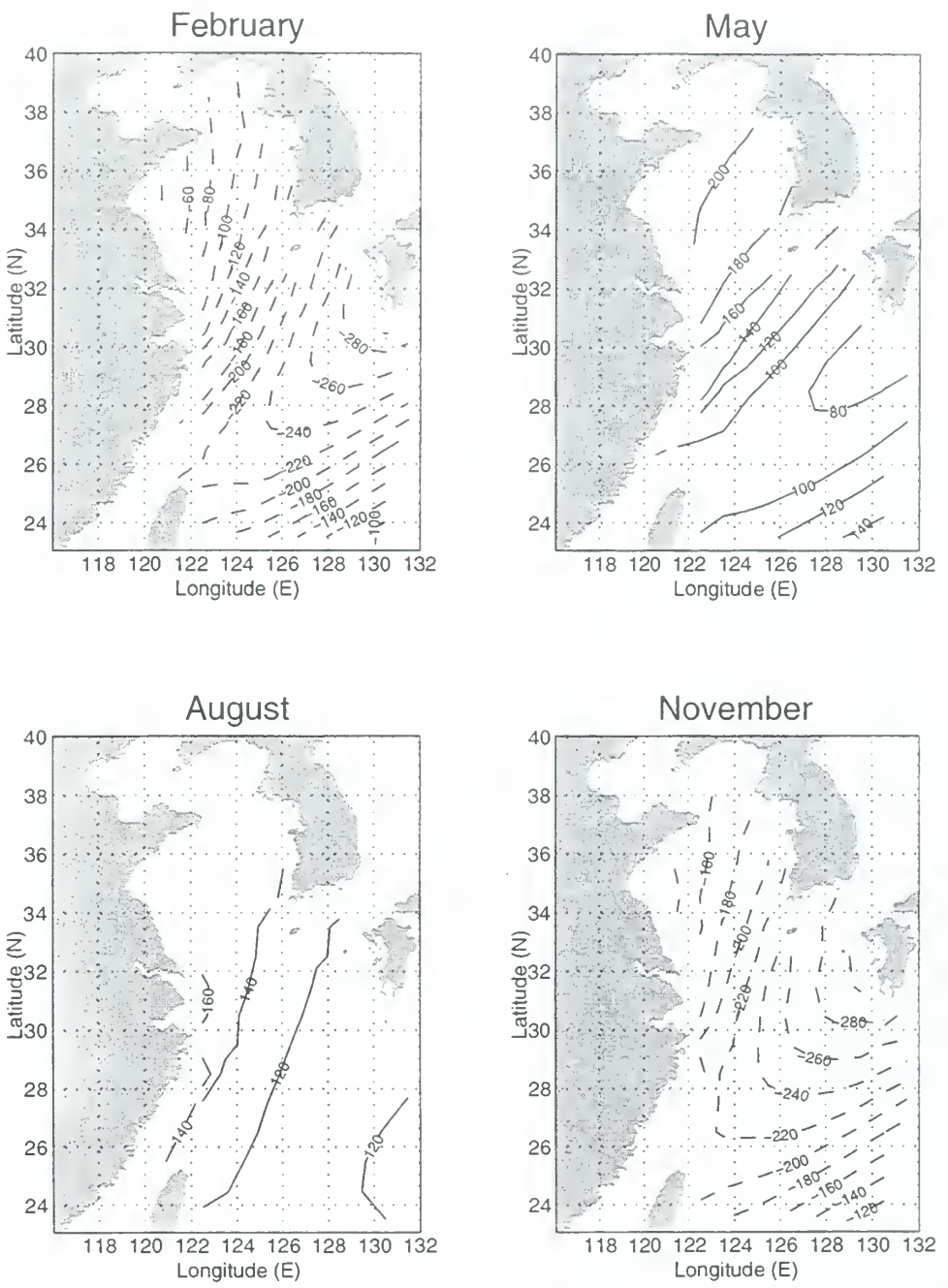

Figure 9. Average net surface heat flux (W m^{-2}) for February, May, August and November. Solid (dashed) lines indicate positive (negative) values.

Month	R_S	R_L	Q_S	Q_L	Q_{net}	Q_S / Q_L
Jan	93.6	78.6	78.3	191.4	-254.8	0.41
Feb	122.0	71.4	64.3	159.3	-173.0	0.40
Mar	165.0	62.4	35.0	116.8	-49.2	0.30
Apr	208.0	51.5	14.0	70.8	71.3	0.20
May	234.8	43.5	5.4	49.5	136.4	0.11
Jun	241.2	34.3	1.5	39.4	166.0	0.04
Jul	269.7	33.1	-2.8	43.7	195.7	-0.06
Aug	257.4	38.4	0.1	72.8	146.1	0.00
Sep	207.5	47.9	8.1	128.6	22.8	0.06
Oct	158.5	62.0	22.4	190.5	-116.6	0.12
Nov	110.5	70.0	43.8	205.5	-208.9	0.21
Dec	89.0	79.3	71.6	212.0	-274.2	0.34
Annual Average	179.7	56.1	28.5	123.4	-28.2	0.23

Table 1. Monthly surface heat flux components obtained from COADS for the ECS. All units are in W m^{-2}.

Month	R_S	R_L	Q_S	Q_L	Q_{net}	Q_S / Q_L
Jan	82.1	88.8	76.8	114.2	-197.7	0.67
Feb	117.6	79.1	53.3	78.7	-93.4	0.68
Mar	172.0	68.5	16.0	44.9	42.6	0.36
Apr	222.3	57.3	0.2	23.2	141.6	0.01
May	261.4	21.1	-1.0	13.6	197.7	-0.07
Jun	260.3	39.0	-1.7	14.4	208.6	-0.12
Jul	247.6	32.4	-2.6	15.8	202.0	-0.16
Aug	245.8	39.1	0.7	57.7	148.3	0.01
Sep	194.3	56.5	8.8	114.8	14.2	0.08
Oct	149.7	73.2	23.2	133.6	-80.3	0.17
Nov	99.7	84.6	48.2	137.6	-170.7	0.35
Dec	75.1	90.7	74.7	137.6	-228.0	0.54
Annual Average	177.3	63.4	24.7	73.8	15.4	0.33

Table 2. Monthly surface heat flux components obtained from COADS for the YS. All units are in W m^{-2}.

Month	R_S	R_L	Q_S	Q_L	Q_{net}	Q_S / Q_L
Jan	81.4	88.8	95.7	172.5	-275.6	0.55
Feb	116.6	79.2	70.8	136.1	-169.4	0.52
Mar	166.5	70.1	32.6	94.4	-30.5	0.35
Apr	212.1	57.0	10.0	51.2	93.9	0.20
May	248.0	48.8	2.9	32.4	163.8	0.09
Jun	241.1	36.0	1.6	24.9	178.5	0.06
Jul	247.2	32.0	-1.3	26.6	189.8	-0.05
Aug	245.4	38.8	2.7	68.7	135.1	0.04
Sep	190.7	51.8	12.4	127.9	-1.3	0.10
Oct	150.4	71.2	29.5	180.6	-130.9	0.16
Nov	103.2	83.7	56.0	192.0	-228.5	0.29
Dec	77.8	91.5	90.3	198.5	-302.5	0.45
Annual Average	173.4	62.4	33.6	108.8	-31.5	0.31

Table 3. Monthly surface heat flux components obtained from COADS for the CB. All units are in W m^{-2}.

Month	R_S	R_L	Q_S	Q_L	Q_{net}	Q_S / Q_L
Jan	93.1	81.6	88.1	233.0	-309.7	0.38
Feb	120.5	74.4	74.3	207.1	-235.4	0.36
Mar	162.6	65.2	44.6	159.6	-106.8	0.28
Apr	206.1	53.7	20.3	104.2	27.9	0.19
May	230.2	44.4	9.9	77.5	98.3	0.13
Jun	238.0	34.6	4.2	57.2	142.1	0.07
Jul	269.9	34.5	-0.2	62.6	172.9	0.00
Aug	254.2	39.0	2.6	88.2	124.3	0.03
Sep	207.5	47.3	9.8	136.5	13.9	0.07
Oct	158.5	62.1	25.9	211.8	-141.3	0.12
Nov	110.9	70.4	47.4	235.6	-242.5	0.20
Dec	89.7	81.6	76.7	249.5	-318.1	0.31
Annual Average	178.4	57.4	33.6	151.9	-64.5	0.18

Table 4. Monthly surface heat flux components obtained from COADS for the TWC. All units are in W m^{-2}.

Month	R_S	R_L	Q_S	Q_L	Qnet	Q_S / Q_L
Jan	99.4	80.5	81.4	248.0	-310.5	0.33
Feb	126.9	73.8	68.9	221.7	-237.6	0.31
Mar	168.5	65.3	43.4	173.9	-114.2	0.25
Apr	211.8	53.7	20.0	118.7	19.5	0.17
May	233.8	44.1	10.5	92.0	87.2	0.11
Jun	243.3	25.1	4.6	67.9	135.7	0.07
Jul	272.9	26.3	1.3	77.3	157.9	0.02
Aug	253.4	39.2	3.3	95.2	115.7	0.03
Sep	213.8	45.6	8.6	130.2	29.4	0.07
Oct	163.3	58.6	24.2	210.0	-129.5	0.12
Nov	116.3	66.7	42.7	238.8	-232.0	0.18
Dec	95.3	78.3	67.6	256.7	-307.2	0.26
Annual Average	183.2	56.4	31.4	160.9	-65.5	0.20

Table 5. Monthly surface heat flux components obtained from COADS for the KC. All units are in W m^{-2}.

The annual variation of net surface heat flux (Figure 10) is nearly sinusoidal and quite similar among the five sub-areas. The YS region leads the rest of the sub-areas by half to one month during the first half of the year, i.e., Q_{net} becomes positive in mid-February in the YS region, in early March in the ECS and CB regions, and in late March in the KC and TWC regions. Q_{net} peaks in June in the YS region and in July in the rest of the sub-areas.

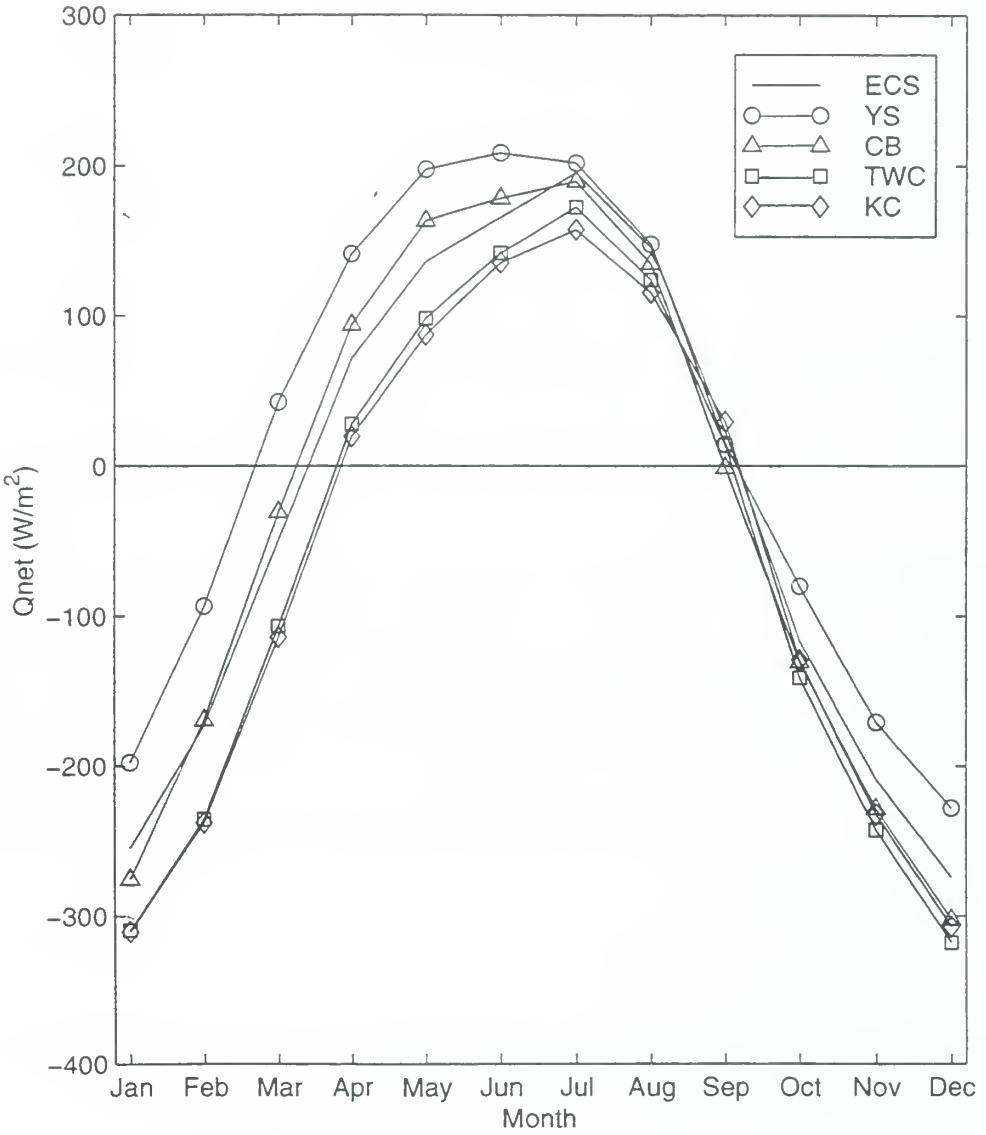

Figure 10. Monthly variation of net surface heat flux for the five regions.

2. Fresh water flux

The surface fresh water flux is the difference between the rate of precipitation (P) and evaporation (E),

$$F = P - E$$

Positive values of F indicate a net water mass gain to the ocean at the surface. The surface fresh water flux exhibits a distinct winter and summer pattern (Figure 11). The summer pattern is characterized by fresh water gain over the whole area, and a saddle-type distribution with two low centers, one in the east (less than 3 cm/month near Kyusyu Island) and another in the west (less than 1 cm/month near the Chinese coast). Centers of high fresh water flux are found in the north (more than 14 cm/month in the northern YS) and in the south (8 cm/month). The winter pattern is characterized by a fresh water loss throughout the whole area, with a maximum water mass loss (19 cm/month in November) near Kyusyu Island.

The monthly variation of surface fresh water budget (Figure 12) shows that E exceeds P during the winter monsoon period (September to March) and P exceeds E during the summer monsoon period (May to August). The shallow water regions (YS, ECS, CB) lead the relatively deep regions (KC, TWC) by nearly one month. F peaks in July in the YS sub-area and in June elsewhere.

3. Surface Buoyancy Flux

Both Q_{net} and F are in-phase during the seasonal variation: positive (negative) values during summer (winter) monsoon season. Thus, the surface buoyancy flux,

$$B = \frac{\alpha g Q_{net}}{\rho_w c_{pw}} + \beta g (P - E) S_0$$

should have a similar seasonal variation as Q_{net} and F. Here, g is the earth gravitational acceleration, ρ_w the characteristic water density, c_{pw} the water specific heat under constant pressure, α the water thermal expansion coefficient, β the salinity contraction coefficient, and S_0 the surface salinity. The surface buoyancy flux B for the five sub-regions has a similar quasi-sinusoidal seasonal variation with the maximum buoyancy gain (loss) in the summer (winter), which results in a shallow (deep) mixed layer in summer (winter).

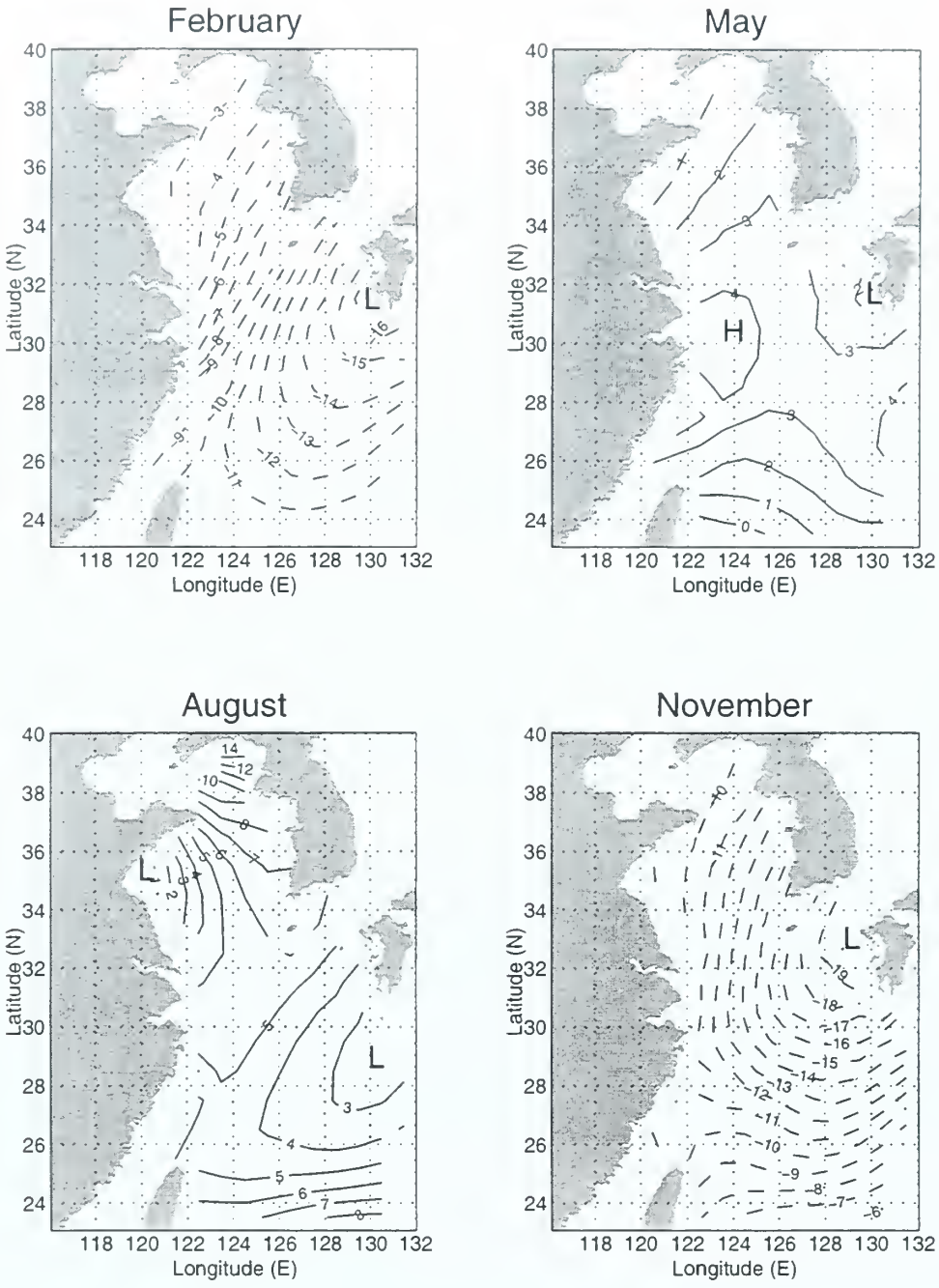

Figure 11. Average surface fresh water flux (cm/month) for February, May, August and November from COADS. Solid lines indicate positive (P>E) values, dashed lines P<E.

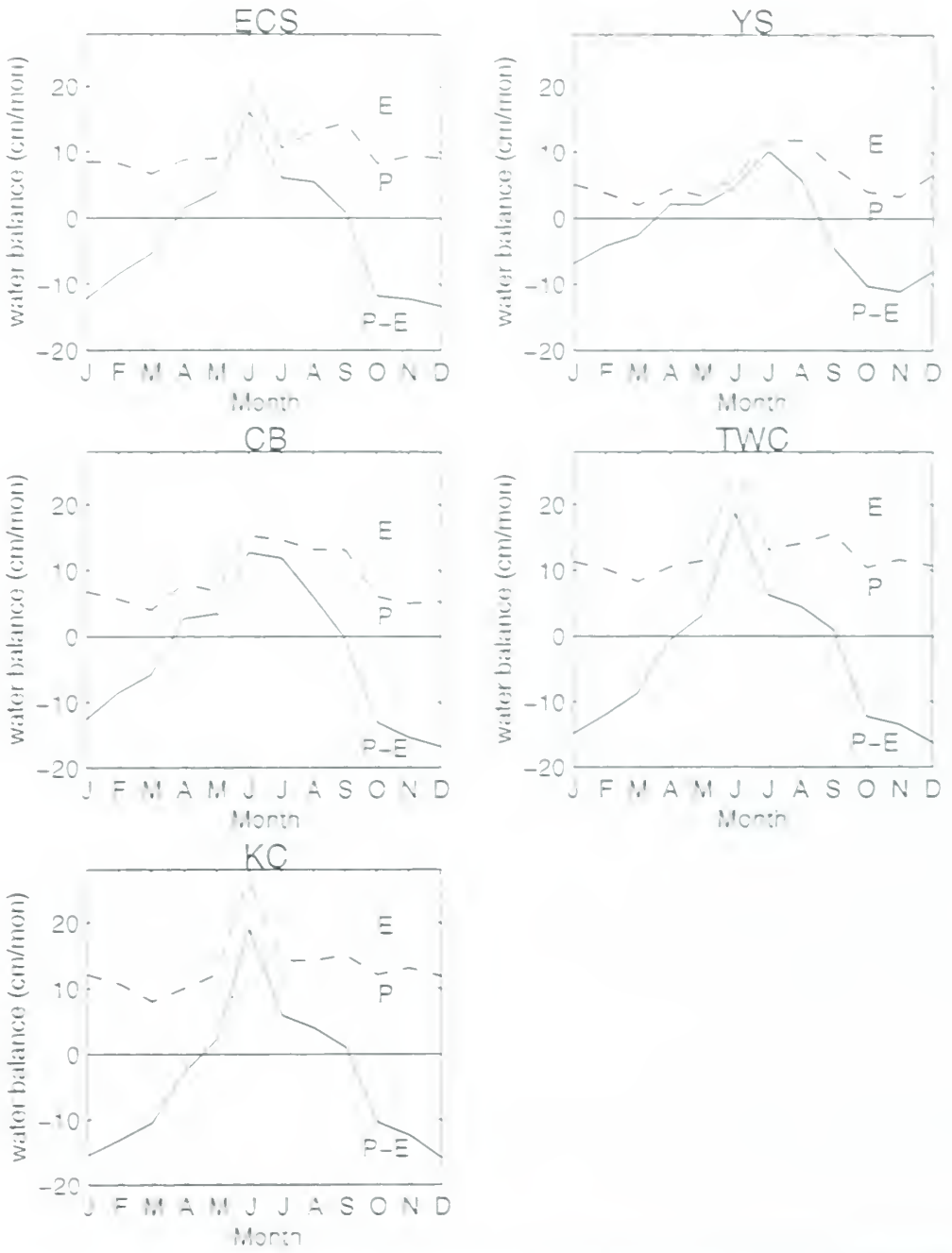

Figure 12. Monthly variation of the surface fresh water budget for the five regions.

IV. THE HYDROGRAPHIC DATA SET

The MOODS is a compilation of observed ocean data worldwide consisting of (a) temperature-only profiles; (b) both temperature and salinity profiles, (c) sound-speed profiles, and (d) surface temperatures from drifting buoys. These measurements are, in general, irregular in time and space. In this study, we analyze temperature and salinity profiles measured from a variety of instruments. Due to the shear size (more than six million profiles) and enormous influx of data to NAVOCEANO from various sources, quality control is a difficult task (Chu et al., 1997c).

Our study domain lies inside the area 24° to 40°N and 118° to 132°E (Figure 13); the data set within this region consisted of nearly 24,000 profiles after rejecting certain data during quality control. These primary editing procedures included removal of profiles with obviously erroneous location, profiles with large spikes, and profiles displaying features that do not match the characteristics of surrounding profiles. In shallow water, this procedure can be partially automated but also involves subjective interpretation because of the under-sampling of MOODS compared to the spatial and temporal variability of the water masses (Chu et al., 1997b).

The main limitation of the MOODS data is its irregular distribution in time and space. Certain periods and areas are over sampled while others lack enough observations to provide meaningful insights. Vertical resolution and data quality are also highly variable depending much on instrument type and sampling expertise. A prominent data sparse area is located off the eastern coastal region of China (Figure 13). The twelve year period of 1975 to 1986 is

found to have a relatively large number of profiles (Figures 14a and b). Yearly temperature (salinity) casts above 2,000 (400) are 1975, 1976, 1978, 1981, and 1986. Within a given year temporally uneven distributions can be seen such as in the 1984 temperature casts (Figure 14c) and salinity casts (Figure 14d). Spatial and temporal irregularities along with the lack of data in certain regions must be carefully weighed in order to avoid statistically-induced variability (Chu et al.,1997c).

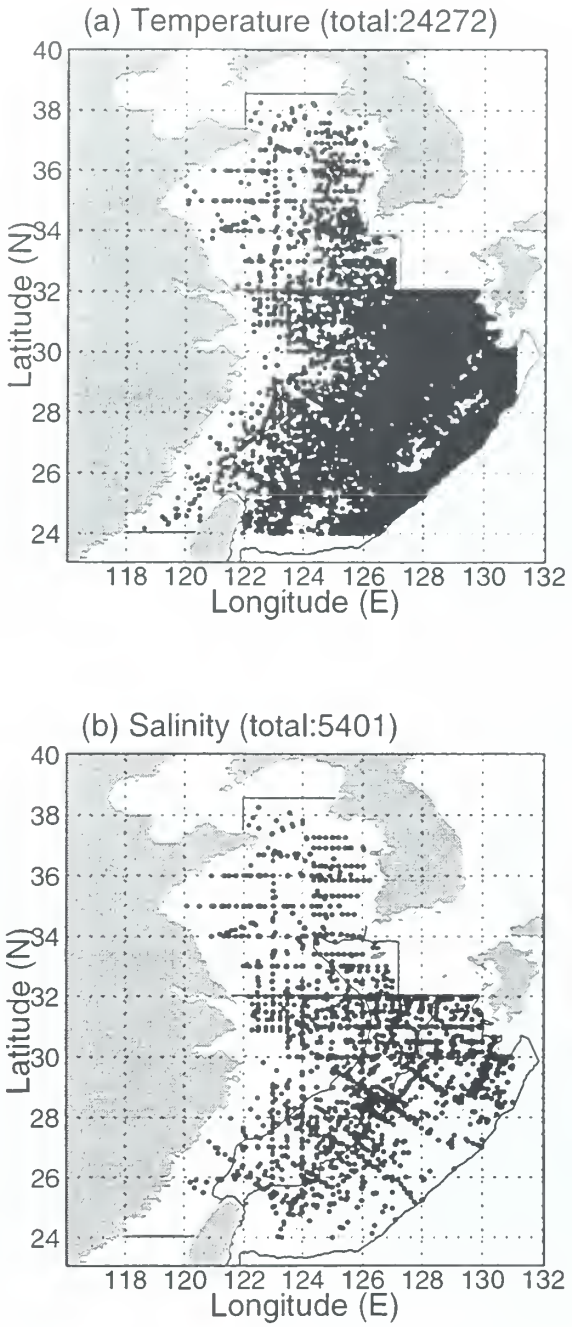

Figure 13. Spatial distribution of MOODS (a) temperature and (b) salinity data during 1975 - 1986.

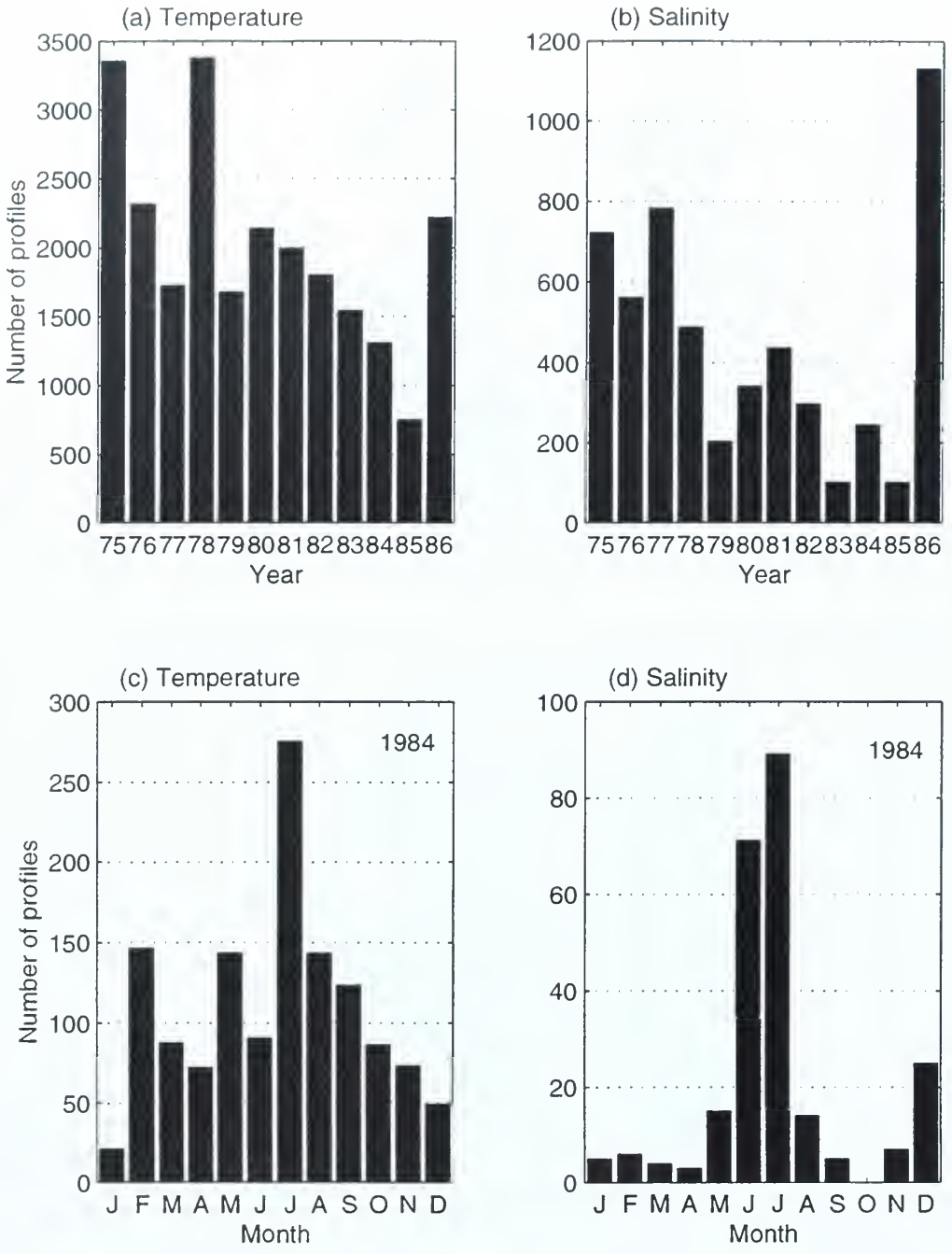

Figure 14. Temporally irregular observation distribution: (a) yearly temperature, (b) yearly salinity, (c) monthly temperature in 1984, and (d) monthly salinity in 1984 for the region shown in Figure 13.

V. SEASONAL VARIATION OF WATER MASS STRUCTURE

A. RELATIVE HEAT STORAGE

Following Artegiani et al. (1997), we used the relative heat storage (RHS) to partition our hydrographic dataset on a seasonal basis. The definition of RHS is taken from Hecht et al. (1985):

$$RHS = \frac{D}{H}\int_{-H}^{0} c_p \rho (T - T_0) dz, \qquad if \quad H < D$$

$$RHS = \int_{-D}^{0} c_p \rho (T - T_0) dz, \qquad if \quad H \geq D$$

where H is the actual water column depth, D the maximum water depth considered, c_p the specific heat at constant pressure, ρ the in situ density, T the water temperature, and T_0 an arbitrary reference temperature. In our computations D=50 m, c_p and ρ have been computed according to Fofonoff and Millard (1983), T has been derived from our dataset and a climatological data set (Levitus, 1994), and T_0=5°C.

The RHS for the five sub-areas is shown in Figure 15. Two extreme seasons can be clearly identified, namely, winter from January to April, and summer from July to November. We can also define the two transition seasons: spring, consisting of May and June, and fall, consisting of December.

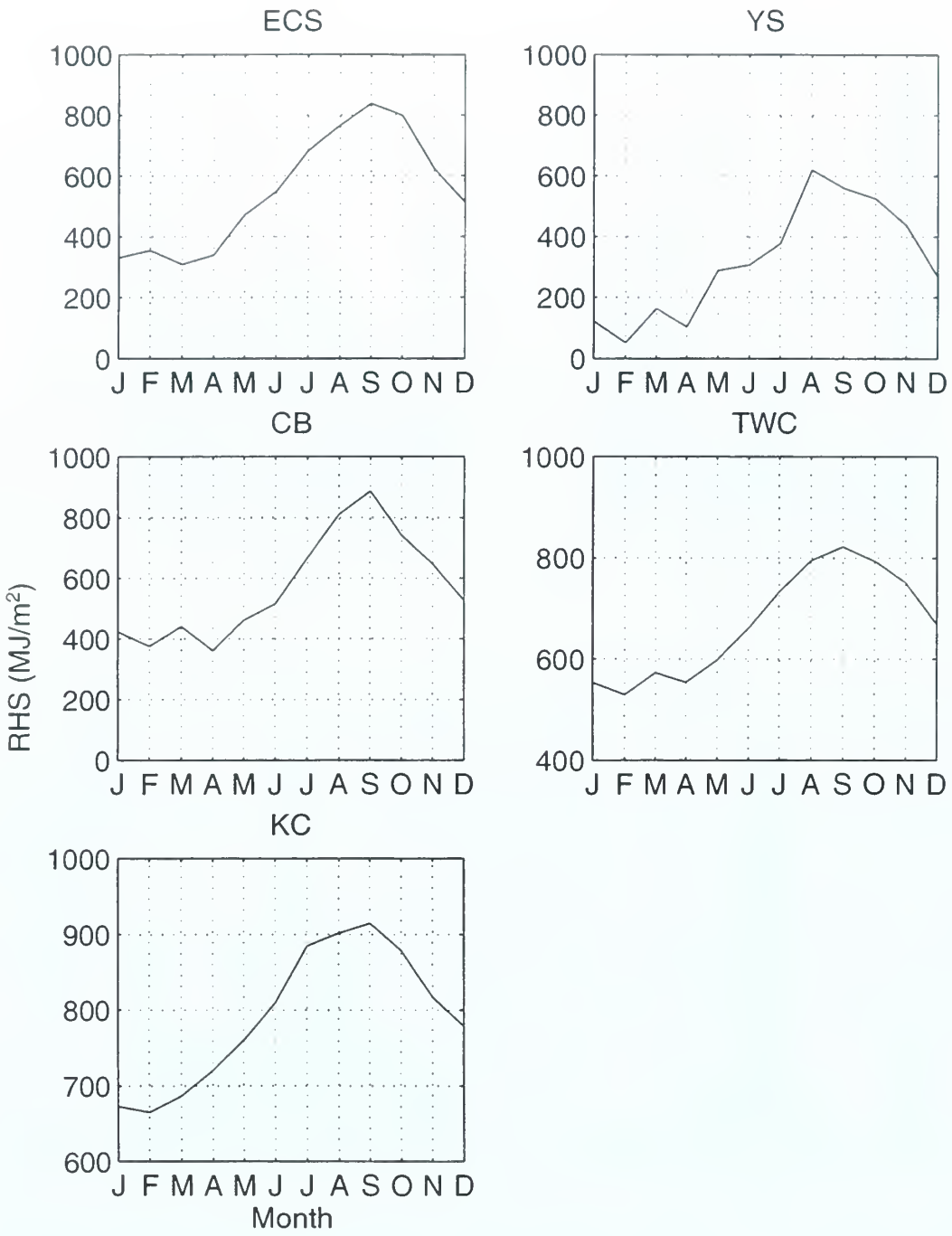

Figure 15. Monthly averaged relative heat storage for the five regions.

B. TEMPERATURE AND SALINITY

The data process is described as follows. First, we binned the profiles into the five sub-regions and four seasons within a year. The temporal resolution becomes a season. Second, we interpolated the profile data into the following depths: 0, 10, 20, 30, 50, 75, 100, 200, 250, 300, 400, 500, 600, 700, 800, 900, 1000, 1100, 1200, 1300, 1400, 1500, 1750, 2000, 2500, 3000, 3500, 4000, 4500, 5000, 5500 m. Third, for a given sub-region and a given season we horizontally averaged the data on each depth. Thus, we established a two dimensional (depth and time) T, S data for each sub-region: $T_n(z_i, \tau_k, t_l)$, and $S_n(z_i, \tau_k, t_l)$, where n refers the sub-region, z_i are the depth grids, τ_k=1975, 1976, ... 1986, is the time sequence in years, and t_l =1, 2, 3, 4, the time sequence within a year in seasons. The first season in the year starts from winter, i.e., t_l =1, represents winter, t_l=2, denotes spring, t_l =3, means summer, t_l=4, refers to autumn. After averaging the data over year,

$$\bar{T}_n(z_i,t_l) \equiv \frac{1}{\Delta\tau}\sum_k T_n(z_i,\tau_k,t_l), \quad \bar{S}_n(z_i,t_l) \equiv \frac{1}{\Delta\tau}\sum_k S_n(z_i,\tau_k,t_l)$$

we obtained the mean seasonal data $\bar{T}_n(z_i,t_l)$ and $\bar{}_n(z_i,t_l)$. Here, $\Delta\tau \equiv$ 12 years (1986-1975+1).

Figures 16, 17 and 18 show the climatological profiles for temperature, salinity and the T-S correlation obtained from our datasets for the five sub-regions. The water mass characteristics of these regions are depicted as follows:

In the ECS shelf region the entire water column exhibits a seasonal thermal cycle (Figure 16a). A well developed thermocline is present down to 30 m depth in spring and extends to the bottom in summer. A significant cooling begins at the end of summer with

immediate effect at the surface and weakening strength with depth. The whole water column becomes well mixed with an isothermal temperature near 18°C in autumn. This is probably due to the entrainment mixing generated by strong surface winds, tidal mixing, and a strong surface buoyancy loss caused by net heat loss of 274 W/m^2 (Table 1) and fresh water loss of 13.3 cm/month. In winter the whole water column is uniformly cooled to 13°C. Total seasonal variability at the bottom is around 6.5°C.

The surface salinity exhibits a minimum value of 32.88 psu in spring which increases to 33.39 psu in summer. It further increases to its maximum value of 34.08 psu in autumn, and then decreases to 33.74 psu in winter (Figure 17a). The surface freshness is in phase with the surface fresh water flux F (Figure 12) and out of phase with the Yangtze River water discharge in such a way that the maximum (minimum) F and the lowest (highest) surface salinity occur in the same season, namely, spring (autumn). However, the surface dilution is out of phase with the Yangtze River discharge. This may confirm an earlier study by Beardsley et al. (1985) which showed that the summer fresh water discharge from the Yangtze River forms a relatively shallow, low salinity plume-like structure extending offshore on average towards the northeast. Thus the dominant factor in determining the near-surface salinity is the surface fresh water flux. In addition, a well developed halocline extends to 30 m in spring and summer, being stronger in spring.

From the T-S diagram (Figure 18a) we can clearly recognize a seasonal layer of East China Sea Surface Water (ECSSW) which corresponds to the relatively low salinities and high temperatures of summer, and an East China Sea Deep Water (ECSDW) layer which is cooled and renewed in winter. From our data, the ECSDW (open circles in Figure 18a) has

average characteristics of T=12.82 °C, S=33.88 psu, and density (σ_t) > 25.2 kg /m^3, which consists with an earlier study by Liu et al. (1992).

In the YS basin the spring-summer thermocline is formed down to the bottom. The bottom water (Figures 16b and 17b) is observed as a low temperature and moderately-high salinity water with a weak seasonal variation. The winter density (σ_t) is greater than 25.6 kg /m^3. These values are consistent with many earlier studies (Li and Yuan, 1992; Chen et al., 1994; Tomczak and Godfrey, 1994) describing the characteristics of the Yellow Sea Cold Water (YSCW) near the bottom all year round. The lack of seasonality might be due to the semi-enclosed basin and the bowl-type bottom topography (Figure 1) which limits mixing with the shallower waters. The surface waters are freshest in summer (S=31.42 psu) but rapidly achieve their saltiest condition in autumn (S=32.98 psu). The net surface fresh water flux has the maximum value (4.84 cm/month) in spring, decreases to a value of -1.96 cm/month in summer (July-November), and continues to drop to the minimum value of -7.96 cm/month in autumn. Such a mismatch between surface salinity and F may suggest that the dominant factor for determining the near surface salinity structure in summer is the river run-off. This coincides with Chen et al.'s (1994) results based on hydrographic observations during 1986. From the T-S diagram (Figure 18b) we can clearly recognize a seasonal variation of the Yellow Sea Cold Water Mass (YSCWM), which is cooled and renewed in winter. We can define the YSCWM as having the winter characteristics of T=6.5°C, S=32.75 psu, and density (σ_t) > 25.6 kg/m^3. These values are consistent with an earlier study by Liu et al. (1992).

In the CB region, there is a strong seasonal variation. A spring-summer thermohaline

is present but weak (Figures 16c and 17c). From summer to autumn, a significant cooling takes place close to the surface and weakens with depth. The whole water column becomes well mixed with a temperature near 17.0°C in autumn. In winter the whole water column is uniformly cooled to 14.3°C. Total seasonal variability at the bottom is around 5.7°C. The surface salinity has a minimum value of 31.46 psu in summer and increases to 33.99 psu in autumn. It further increases to the maximum value of 34.41 psu in winter, and then decreases to 32.68 psu in spring (Figure 17c). Total seasonal haline variability at the bottom is around 1.69 psu. Figure 2 indicates that the TWC bifurcates near the CB region into the Yellow Sea Warm Current and the Tsushima Current. There should be some connection between the CB region and the upper layer (30 m) of the TWC region. However, the similarity between CB and the upper TWC profiles only occurs in temperature (Figures 16c and 16d) but not in salinity. The seasonal surface salinity variation follows the seasonal F: minimum salinity and maximum surface fresh water flux in summer and vice versa in winter. From T-S diagram (Figure 18c) we can clearly recognize the TWC deep water (TWCDW) and YESMW.

In the TWC region the upper water column (surface to 60 m), usually called the TWC Upper Water (TWCUW), exhibits a seasonal thermohaline cycle (Figures 16d and 17d). Total seasonal variability of temperature (salinity) is around 7°C (1.02 psu) at the surface and weakens with depth. Below the 60 m depth there exists a permanent thermocline with a very weak seasonal variation. At the bottom (150 m), the water properties are seasonally invariant; the temperature is about 15°C, and the salinity is around 34.62 psu. In winter, the surface waters are coolest with a temperature of 19°C. Significant warming begins in spring with a 4.0°C increase from winter conditions followed by a 3.0°C increase

from spring to summer. In summer, the surface temperature reaches its maximum of 26.3 °C. Significant cooling (4.7 °C) occurs in autumn. The surface salinity has the minimum value of 33.67 psu in summer and increases to the maximum value of 34.69 psu in autumn. It slightly decreases to 34.52 psu in winter and then decreases to 33.91 psu in spring. The surface freshness is in phase with the surface fresh water flux F (Figure 12). From the T-S diagram (Figure 18d) we can clearly recognize a seasonal layer in the TWC which corresponds to the relatively fresh and warm water in summer and the saline and cool water in winter.

In the KC region the upper water column (surface to 80 m), usually called the Kuroshio Surface Water (KSW), exhibits a seasonal thermal cycle (Figures 16e,f; 17e,f). Total seasonal variability of temperature (salinity) is around 5.7°C (0.47 psu) at the surface and weakens with depth. From 80 to 600 m there exists a permanent thermocline/halocline with a very weak seasonal variation. At 1000 m depth, the temperature is about 3.7°C and the salinity is around 34.43 psu. In winter, the surface has a minimum temperature of 21.7°C. A significant warming begins in spring. There is a 3.7°C increase from winter to spring and a 2.0°C increase from spring to summer. In summer, the surface temperature reaches its maximum of 27.4°C. A significant cooling starts in autumn. The surface salinity has the minimum value of 34.29 psu in summer, increases to the maximum value of 34.75 psu in winter, and then decreases to 34.56 psu in spring. The surface freshness is in-phase with the surface fresh water flux F (Figure 12). Our data also shows the existence of S-type salinity profiles with a maximum salinity in the layer between 150 and 250 m, which is associated with the Kuroshio Sub-Surface Water (KSSW); and a minimum salinity at a 600

m depth, which is associated with the Kuroshio Intermediate Water (KIW). In the sublayer between 150 and 450 m, the salinity decreases with depth. From the T-S diagram (Figure 18e) we can clearly recognize a seasonal layer in the KC, which corresponds to the relatively fresh and warm water in summer and saline and cool water in winter.

Putting five T-S diagrams (Figures 18a-e) into one T-S diagram, the five sub-regions and various ECS/YS water masses are well represented (Figure 19). We can see the connections and mixing of water masses among the five sub-regions. For example, the water masses in the CB region come from TWCDW, YEMW, and YSMW. The YS and ECS waters are mixed during spring and summer. Besides, various ECS/YS water masses are well classified on this T-S diagram.

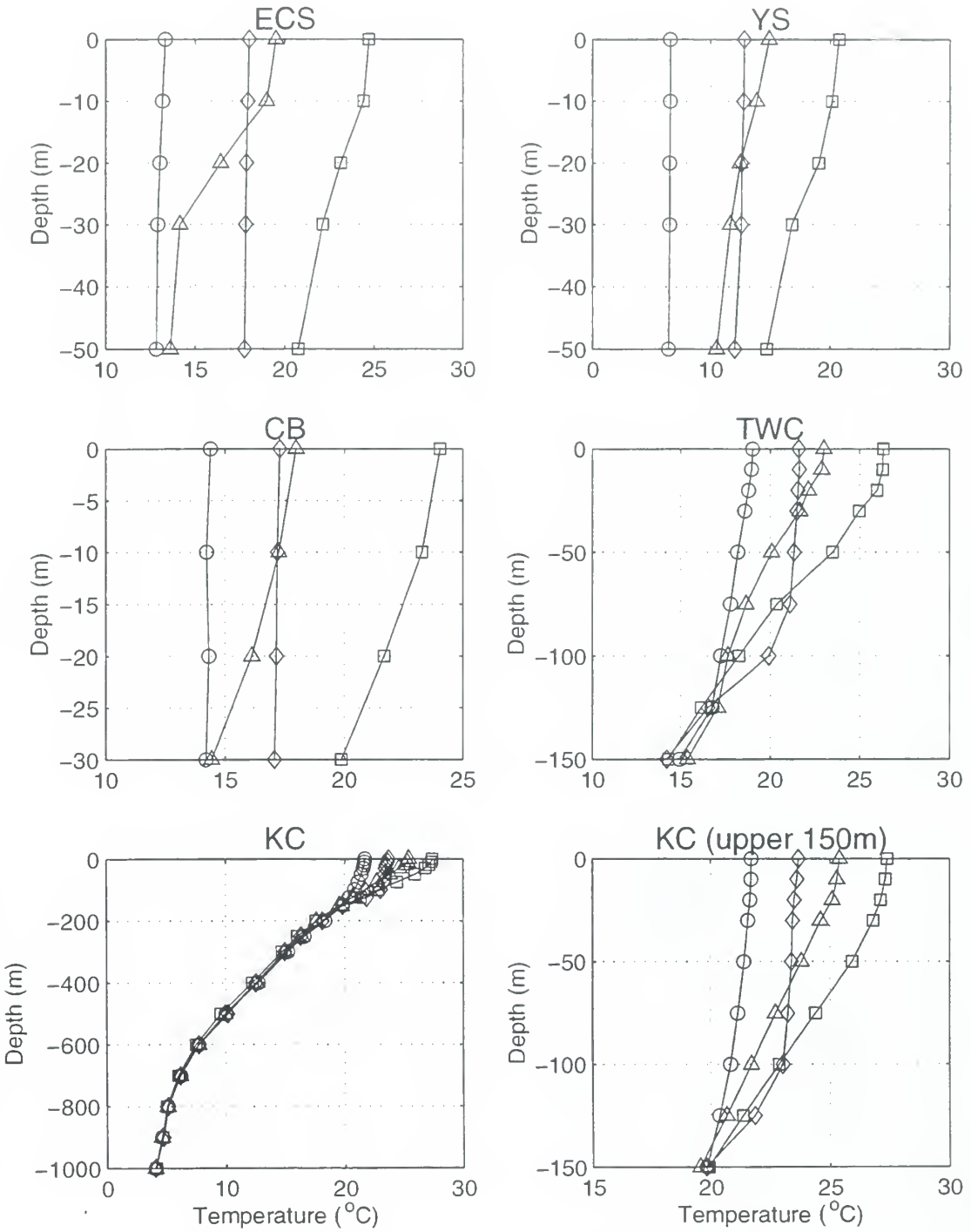

Figure 16. Climatological profiles of temperature (°C) for (a) ECS, (b) YS, (c) CB, (d) TWC and (e) KC. Symbols indicate winter (○), spring (Δ), summer (□) and autumn (◇).

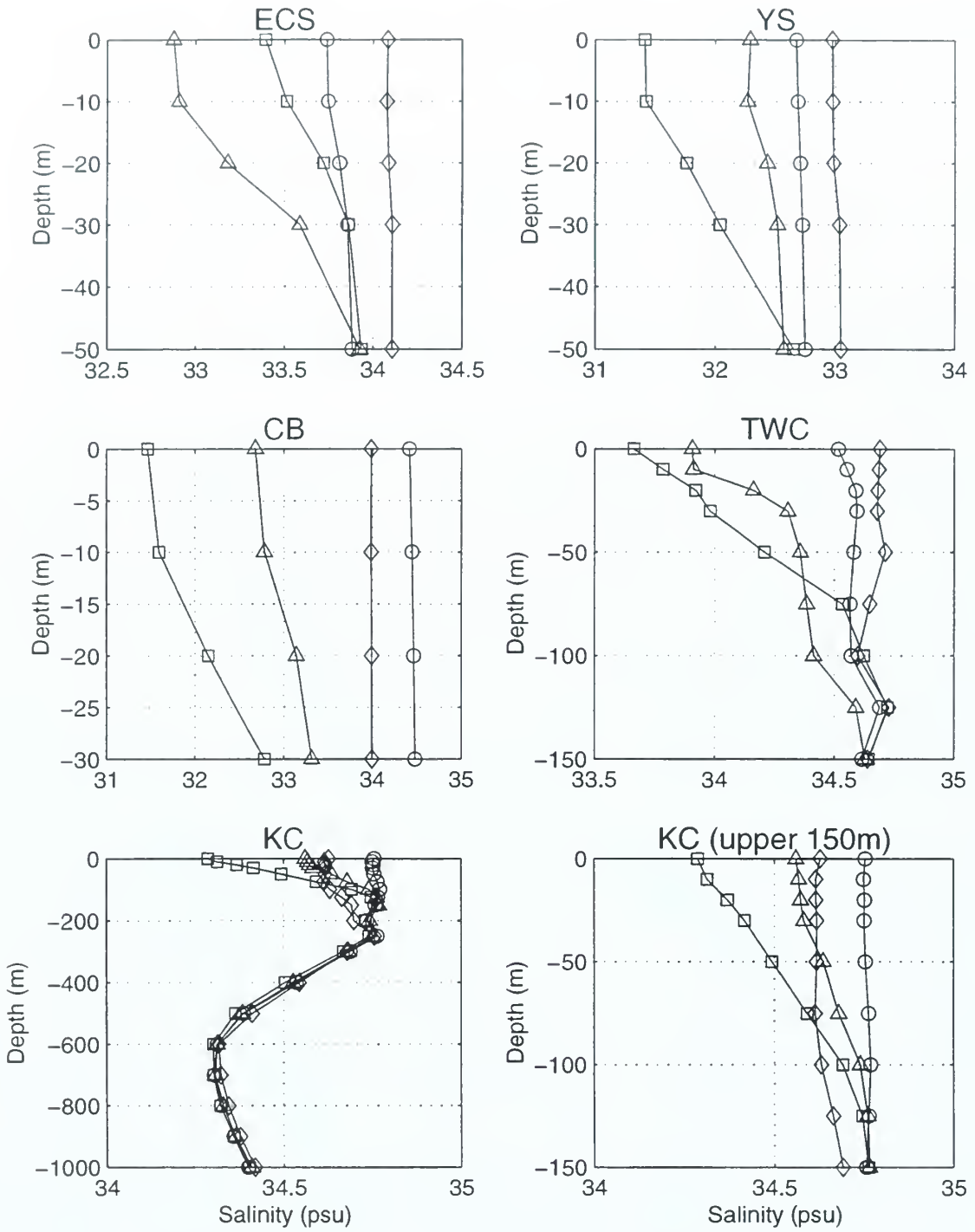

Figure 17. Climatological profiles of salinity (psu) for (a) ECS, (b) YS, (c) CB, (d) TWC and (e) KC. Symbols indicate winter (○), spring (Δ), summer (□) and autumn (◊).

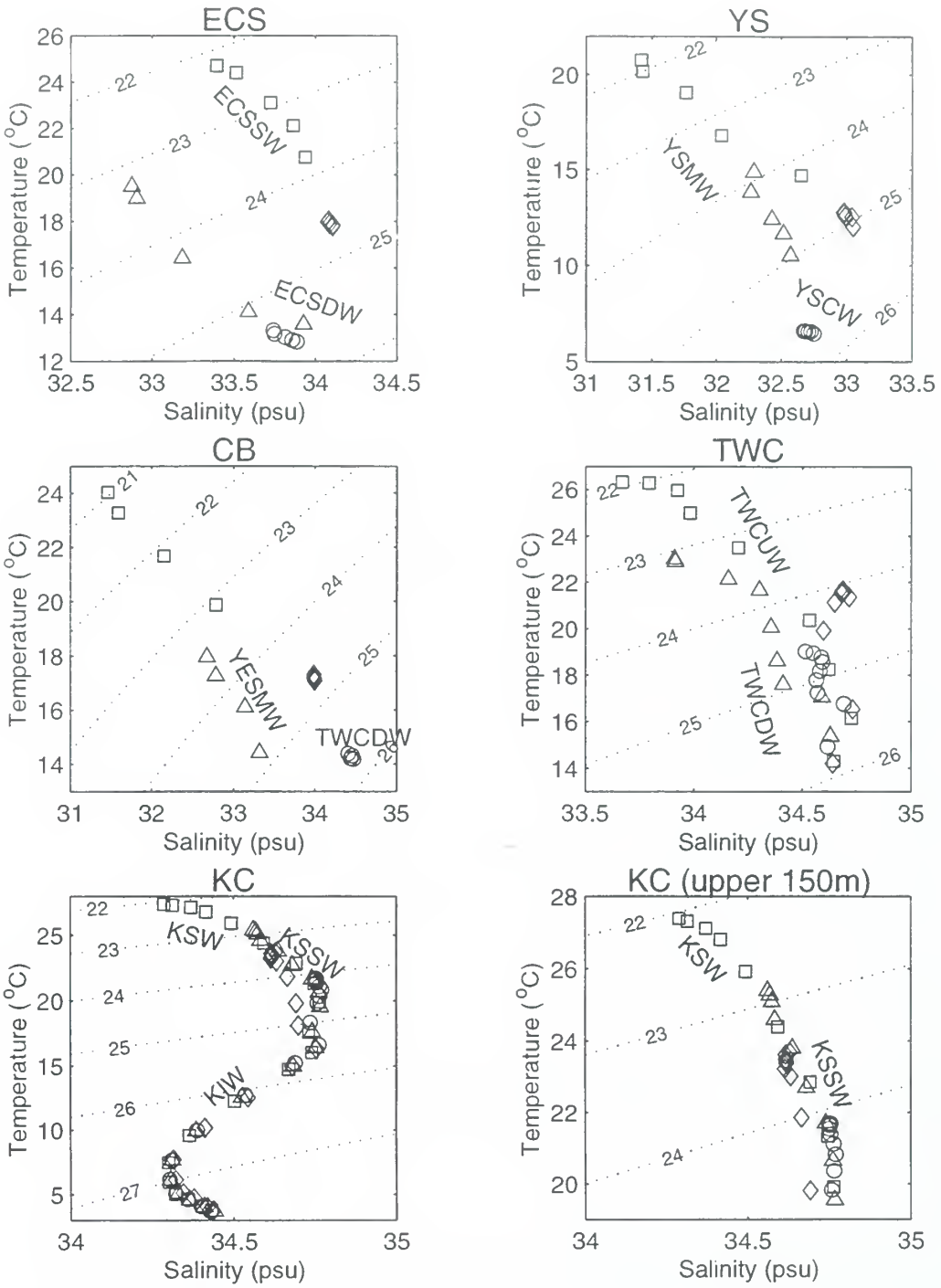

Figure 18. Climatological T-S diagrams for (a) ECS, (b) YS, (c) CB, (d) TWC and (e) KC. Symbols indicate winter (○), spring (Δ), summer (□) and autumn (◇).

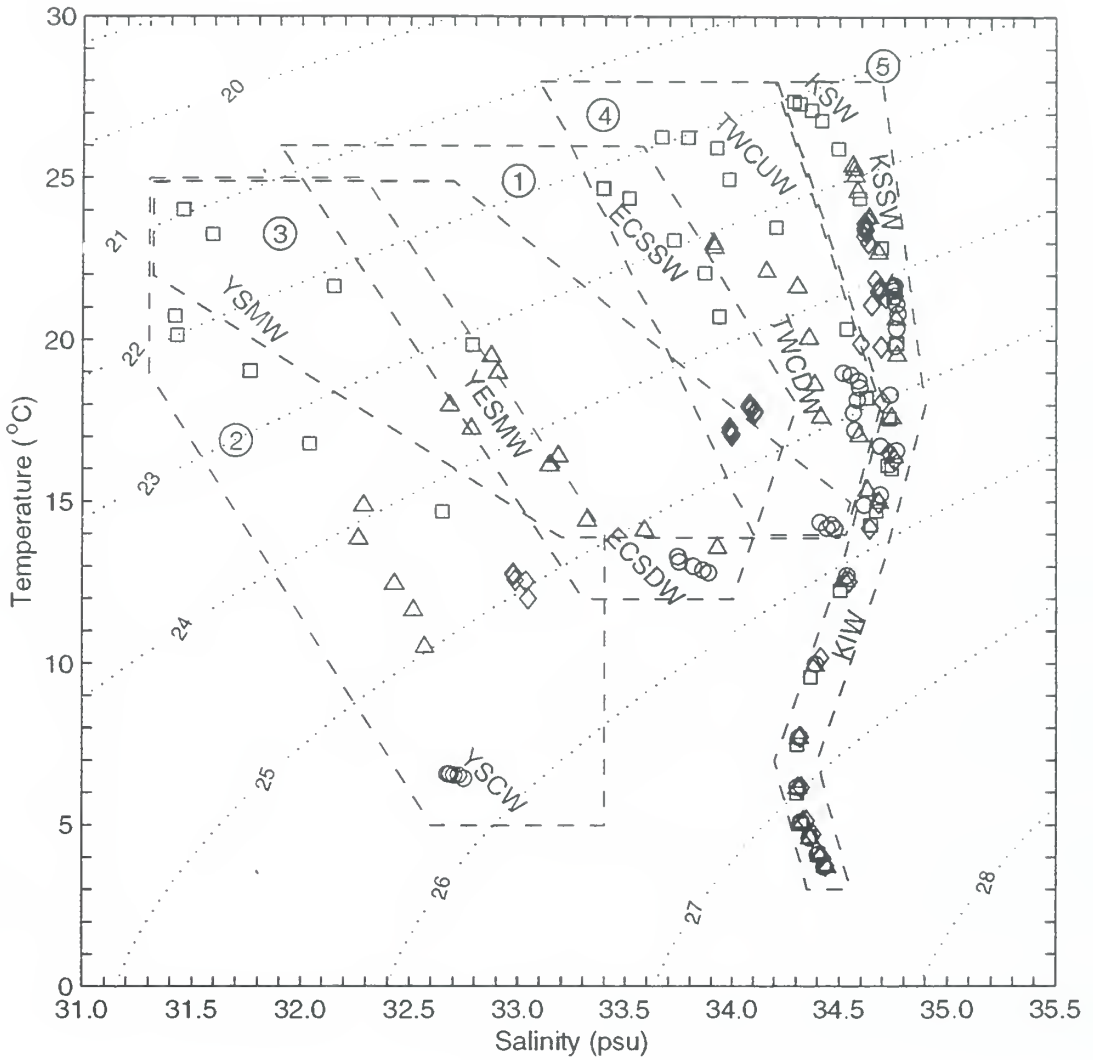

Figure 19. Water mass classification of climatological T-S diagram for ① ECS, ② YS, ③ CB, ④ TWC, and ⑤ KC. Symbols indicate winter (○), spring (Δ), summer (□) and autumn (◇).

VI. INTERANNUAL VARIATION OF THERMOHALINE STRUCTURE

The interannual variability of T, S features can be obtained by subtracting the mean seasonal signals [$\bar{T}_n(z_i,t_l), \bar{S}_n(z_i,t_l)$] from [$T_n(z_i,\tau_k,t_l), S_n(z_i,\tau_k,t_l)$],

$$\hat{T}_n(z_i,\tau_k,t_l) = T_n(z_i,\tau_k,t_l) - \bar{T}_n(z_i,t_l), \quad \hat{S}_n(z_i,\tau_k,t_l) = S_n(z_i,\tau_k,t_l) - \bar{S}_n(z_i,t_l).$$

Figures 20-24 show the interannual variations of $\hat{T}_n(z_i,\tau_k,t_l)$ and $\hat{S}_n(z_i,\tau_k,t_l)$ at three different levels for each sub-region. Owing to the irregularity of the MOODS data, there might be no data in a given sub-region for some seasons. For example, there is no data in the YS in 1978 and 1985. We should be very cautious when interpreting the interannual variability from this dataset.

In the ECS shelf region, the temperature anomaly ($\hat{T}_n$) has a maximum value of 3.4°C at the surface in spring 1980 and a minimum value of -3.3°C at the surface in spring 1979. The salinity anomaly ($\hat{S}_n$) has a maximum value of 1.87 psu at the surface in spring 1977 and a minimum value of -1.78 psu at the surface in spring 1984 (Figure 20). The modest ($|\hat{T}_n| > 2$°C, $|\hat{S}_n| > 1$ psu) and strong ($|\hat{T}_n| > 3$°C, $|\hat{S}_n| > 1.5$ psu) anomalies occur in spring and summer seasons (Tables 6-7). For example, a strong warming and salting process occurs in spring 1977, and a strong freshen and modest cooling process occurs in spring 1984.

In the YS region, the temperature anomaly has a maximum value of 6.0°C at the 50 m depth in summer 1979 and a minimum value of -8.5°C at the 20 m depth in summer 1984.

The salinity anomaly has a maximum value of 1.03 psu at the surface in spring 1976 and a minimum value of -2.84 psu at the surface in spring 1982 (Figure 21). A strong freshening and modest warming process occurs in spring 1982 (Tables 8-9).

In the CB region, the temperature anomaly has a maximum value of 6.2°C at the 30 m depth in summer 1981 and a minimum value of -3.1°C at the surface in spring 1983. The salinity anomaly has a maximum value of 1.89 psu at the surface in spring 1980 and a minimum value of -1.33 psu at the 30 m depth in summer 1977 (Figure 22). A very strong warming occured in summer 1981 (Table 10). The years of 1970s were characterized as the freshening period and the years of 1980s were featured as the saline period (Table 11).

In the TWC region, the temperature anomaly has a maximum value of 3.0°C at the 50 m depth in spring 1977 and a minimum value of -3.5°C at the surface in spring 1983. The salinity anomaly has a maximum value of 0.82 psu at the surface in summer 1979 and a minimum value of -1.26 psu at the surface in summer 1983 (Figure 23). The fluctuations of the salinity anomaly decreases with depth. Modest and strong anomaly periods are listed in Tables 12-13.

In the KC region, the temperature anomaly has a maximum value of 1.8°C at the 150 m depth in autumn 1980 and a minimum value of -1.4°C at the 50 m depth in winter 1986. The salinity anomaly has a maximum value of 0.23 psu at the 150 m depth in autumn 1975 and a minimum value of -0.35 psu at the surface in summer 1982 (Figure 25).

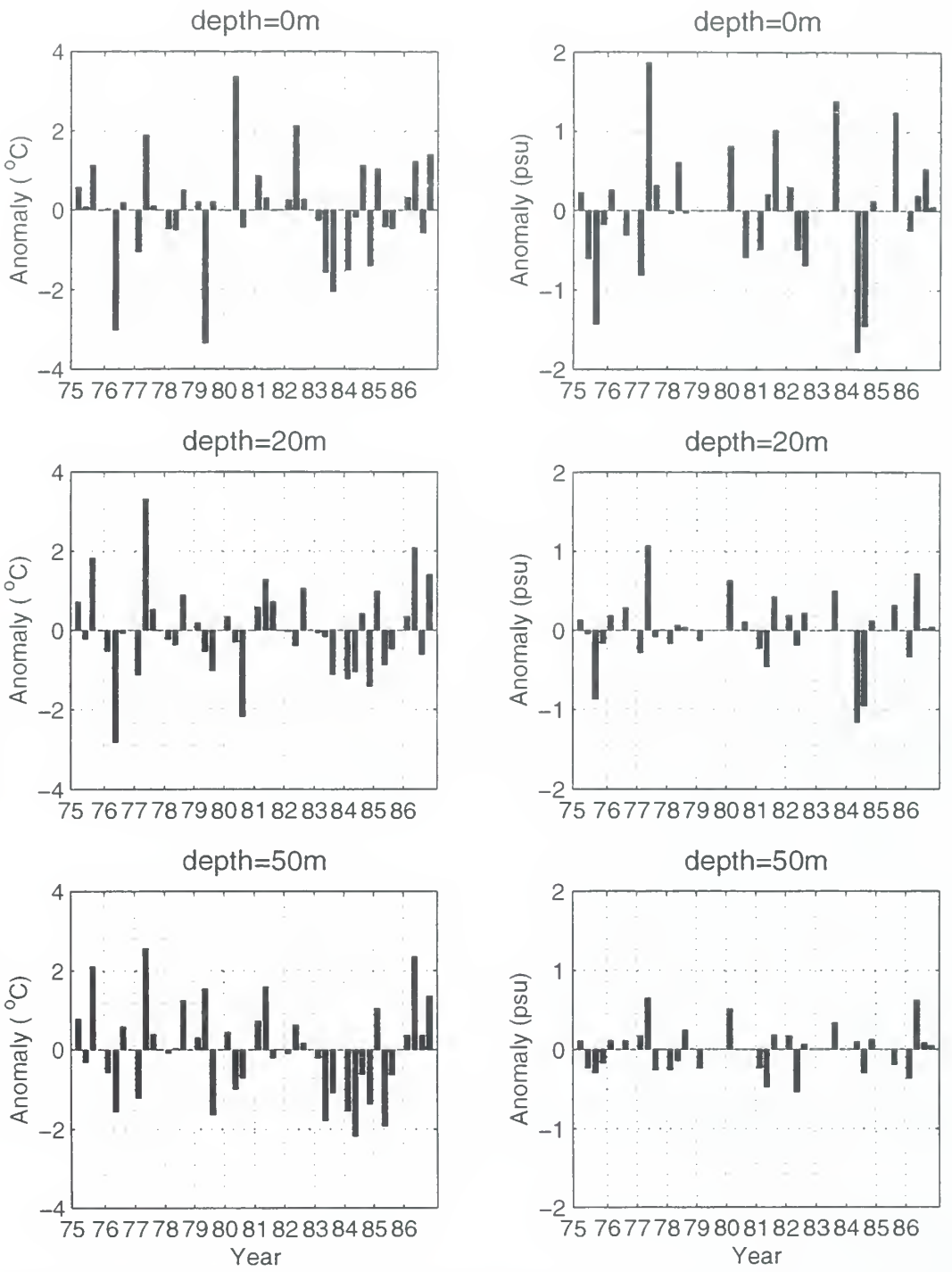

Figure 20. Interannual variation of temperature and salinity anomalies for the ECS shelf at different depths: (a) surface, (b) 20 m, and (c) 50 m.

Anomaly periods	Above 1.0 °C	Above 1.5 °C
Warm	summer 75 (50 m) spring 77 (20 m, 50 m) spring 80 (0 m) spring 82 (0 m) spring 86 (20, 50 m)	spring 77 (20 m) spring 80 (0 m)
Cold	spring 76 (0, 20 m) spring 79 (0 m) summer 80 (20 m) summer 83 (0 m) spring 84 (50 m)	spring 76 (0 m) spring 79 (0 m)

Table 6. Warm and cold anomaly periods for ECS.

Anomaly periods	Above 1 psu	Above 1.5 psu
Salty	spring 77 (0, 20 m) summer 81 (0 m) summer 83 (0 m) summer 85 (0 m)	spring 77 (0 m)
Fresh	summer 75 (0 m) spring 84 (0, 20 m) summer 84 (0 m)	spring 84 (0 m)

Table 7. Salty and fresh anomaly periods for ECS.

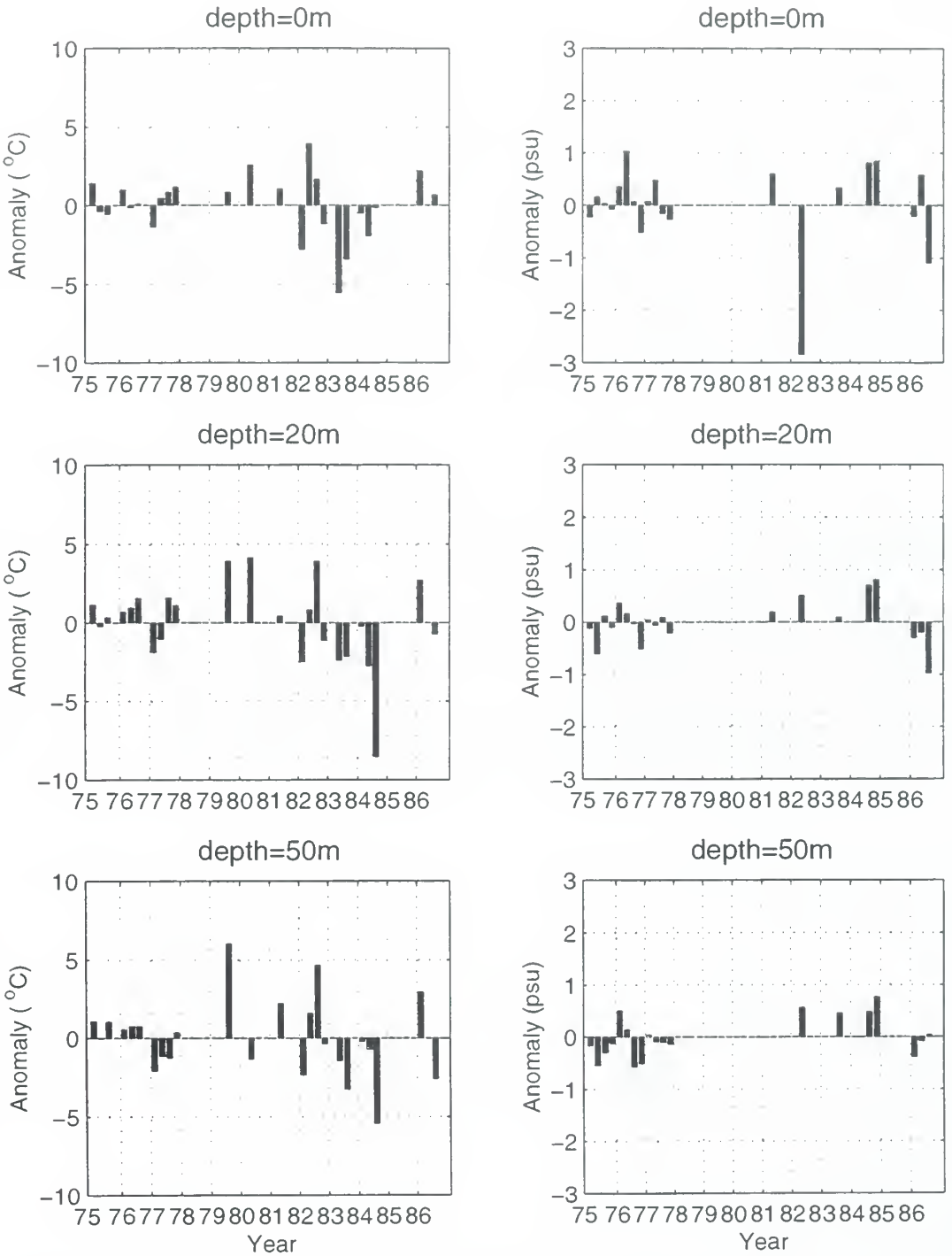

Figure 21. Interannual variation of temperature and salinity anomalies for the YS region at different depths: (a) surface, (b) 20 m, and (c) 50 m.

Anomaly periods	Above 3°C	Above 5°C
Warm	summer 79 (20, 50 m) summer 80 (20 m) spring 82 (0 m) summer 82 (20, 50 m)	summer 79 (50 m)
Cold	spring 83 (0 m) summer 83 (0, 50 m) summer 84 (20, 50 m)	spring 83 (0 m) summer 84 (20, 50 m)

Table 8. Warm and cold anomaly periods for YS.

Anomaly periods	Above 1 psu	Above 1.5 psu
Salty	spring 76 (0 m)	
Fresh	spring 82 (0 m) summer 86 (0 m)	spring 82 (0 m)

Table 9. Salty and fresh anomaly periods for YS.

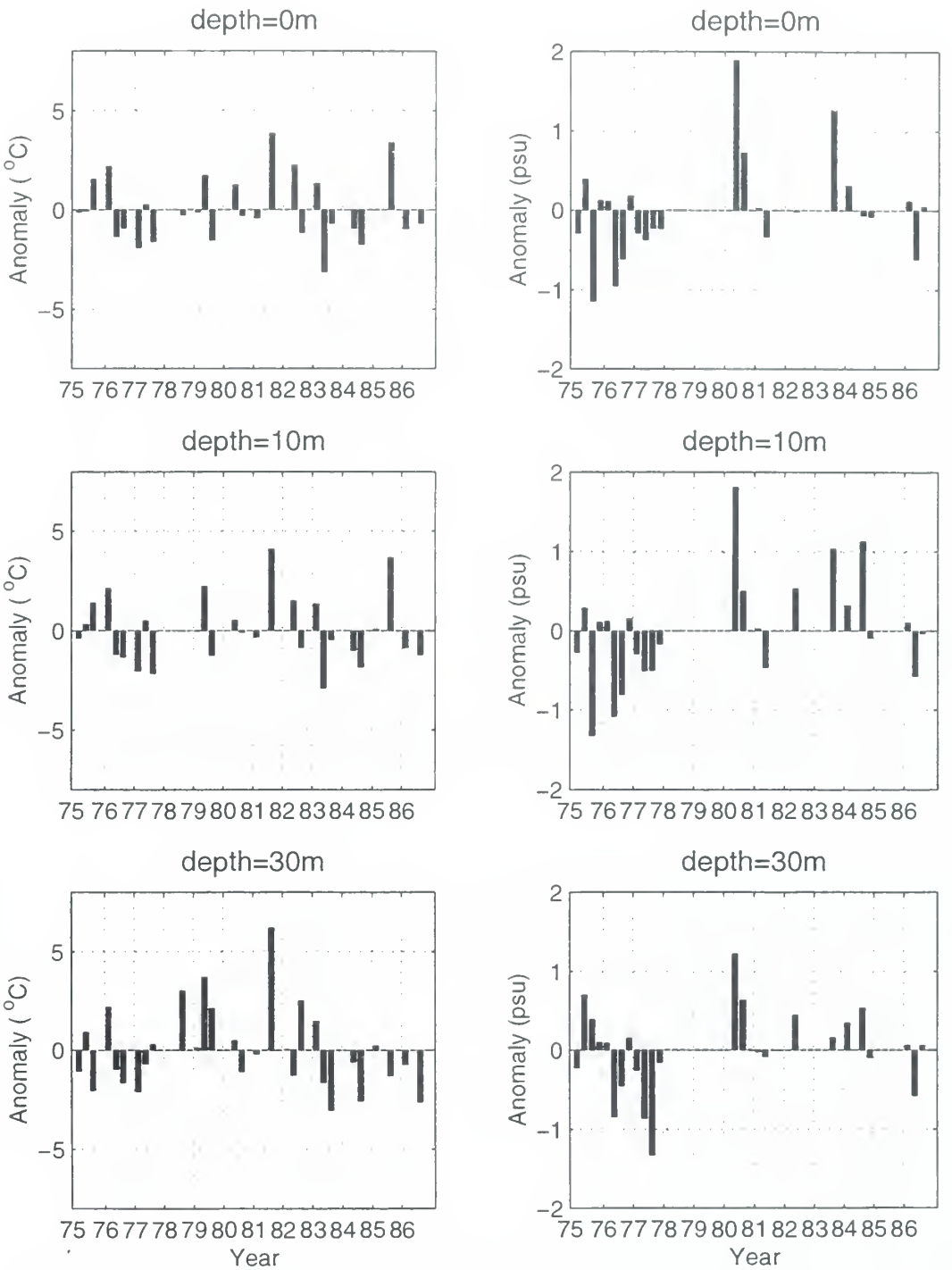

Figure 22. Interannual variation of temperature and salinity anomalies for the CB region at different depths: (a) surface, (b) 10 m, and (c) 30 m.

Anomaly periods	Above 2°C	Above 3°C
Warm	winter 76 (0, 10, 30 m) summer 78 (30 m) spring 79 (10, 30 m) summer 79 (30 m) summer 81 (0, 10, 30 m) spring 82 (0 m) summer 82 (30 m) summer 85 (0, 10 m)	summer 78 (30 m) spring 79 (30 m) summer 81 (0, 10, 30 m) summer 85 (0, 10 m)
Cold	winter 77 (10, 30 m) summer 77 (10 m) spring 83 (0, 10 m) summer 83 (30 m) summer 84 (30 m) summer 86 (30 m)	spring 83 (0 m) summer 83 (30 m)

Table 10. Warm and cold anomaly periods for CB.

Anomaly periods	Above 1.0 psu	Above 1.5 psu
Salty	spring 80 (0, 10, 30 m) summer 83 (0, 10 m) summer 84 (10 m)	spring 80 (0, 10 m)
Fresh	summer 75 (0, 10 m) spring 76 (10 m) summer 77 (30 m)	

Table 11. Salty and fresh anomaly periods for CB.

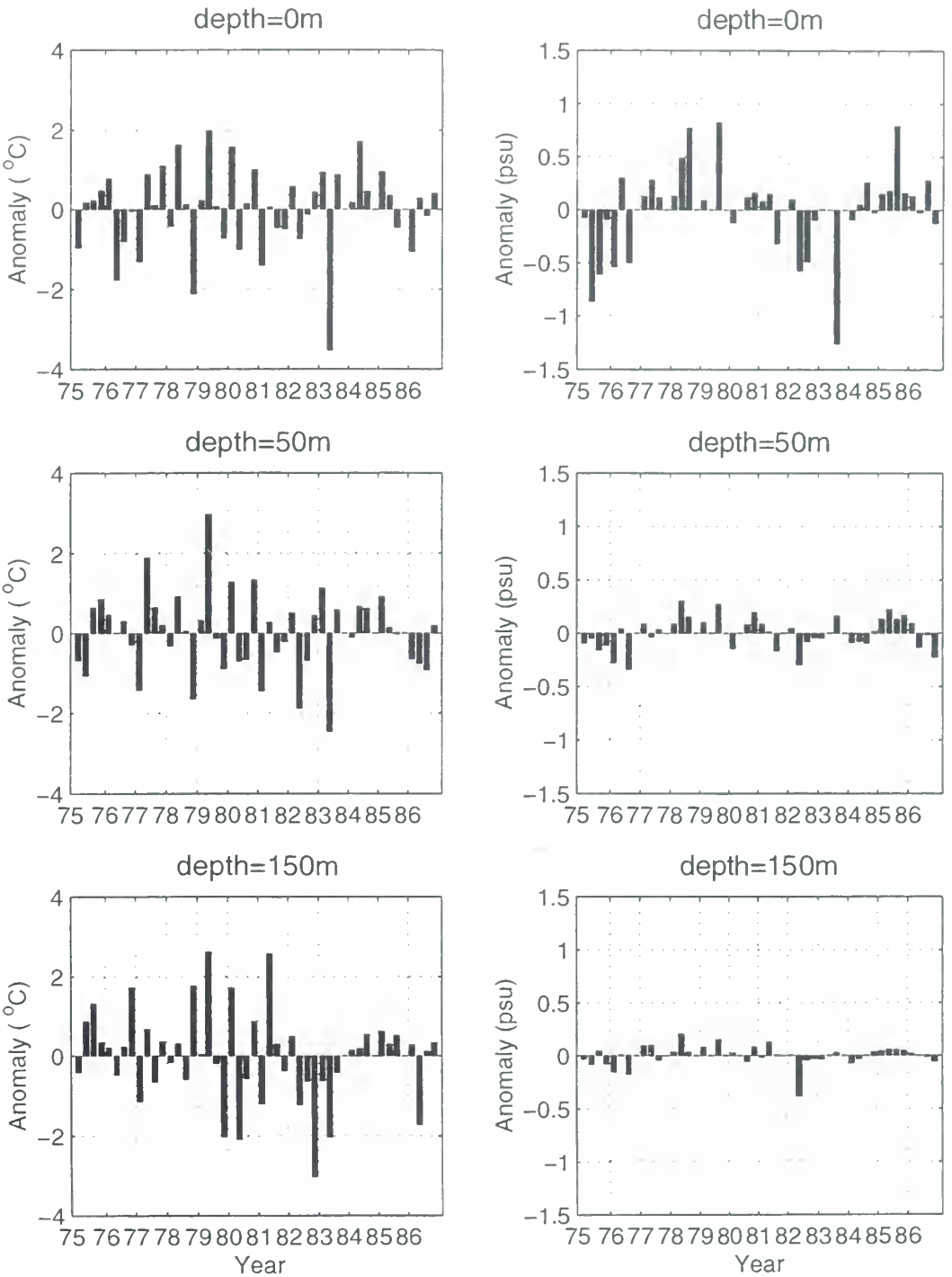

Figure 23. Interannual variation of temperature and salinity anomalies for the TWC region at different depths: (a) surface, (b) 50 m, and (c) 150 m.

Anomaly periods	Above 1.0°C	Above 1.5°C
Warm	spring 77 (0, 50 m) winter 80 (0, 50, 150 m) winter 83 (50 m)	spring 77 (0, 50 m) winter 80 (0, 150 m)
Cold	winter 77 (0, 50, 150 m) summer 77 (150 m) winter 81 (0, 50 m) winter 86 (0 m)	

Table 12. Warm and cold anomaly periods for TWC.

Anomaly periods	Above 0.5 psu	Above 1.0 psu
Salty	summer 78 (0 m) summer 79 (0 m) summer 85 (0 m)	
Fresh	spring 75 (0 m) summer 75 (0 m) winter 76 (0 m) summer 76 (0 m) spring 82 (0 m) summer 83 (0 m)	summer 83 (0 m)

Table 13. Salty and fresh anomaly periods for TWC.

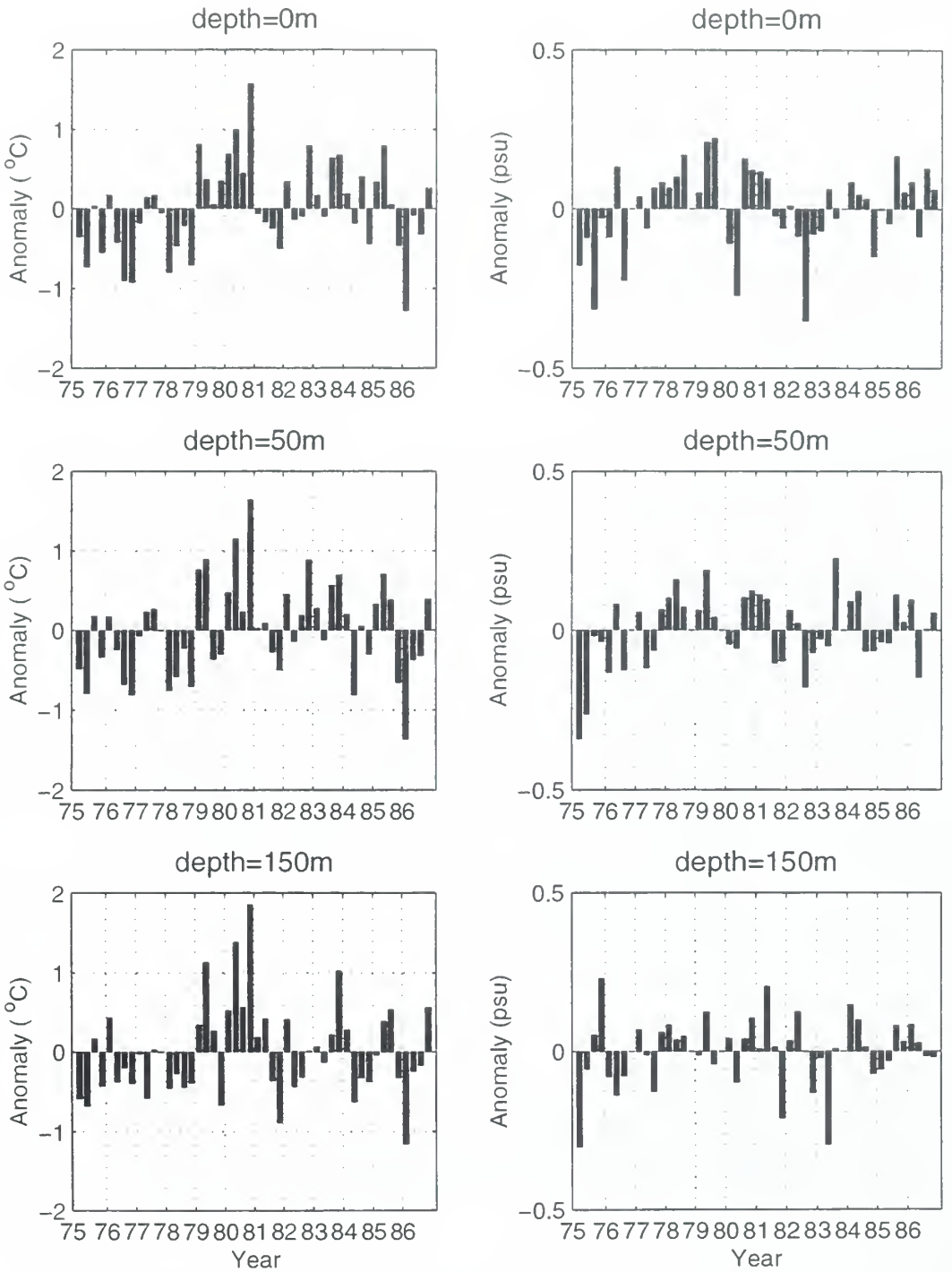

Figure 24. Interannual variation of temperature and salinity anomalies for KC region at different depths: (a) surface, (b) 50 m, and (c) 150 m.

Anomaly periods	Above 1.0°C	Above 1.5°C
Warm	spring 79 (150 m) spring 80 (50, 150 m) autumn 80 (0, 50, 150 m) autumn 83 (150 m)	autumn 80 (0, 50, 150 m)
Cold	winter 86 (0, 50, 150 m)	

Table 14. Warm and cold anomaly periods for KC.

Anomaly periods	Above 0.2 psu	Above 0.3 psu
Salty	autumn 75 (150 m) spring 79 (0 m) summer 79 (0 m) spring 81 (150 m) summer 83 (50 m)	
Fresh	winter 75 (50, 150 m) spring 75 (50 m) summer 75 (0 m) summer 76 (0 m) spring 80 (0 m) autumn 81 (150 m) summer 82 (0 m) spring 83 (150 m)	winter 75 (50 m) summer 82 (0 m)

Table 15. Salty and fresh anomaly periods for KC.

VII. CONCLUSIONS

The work presented here describes the climatological water mass structure of the East China and Yellow Seas. Based on the currents and bathymetry, we divide the area into five sub-regions: the East China Sea shelf, the Yellow Sea basin, the Cheju bifurcation zone, the Taiwan Warm Current area, and the Kuroshio Current area. We use the U.S. Navy's Master Oceanographic Observation Data Set and the Comprehensive Ocean-Atmosphere Data Set to investigate the linkage between the fluxes (momentum, heat, and moisture) across the air-ocean interface and the formation of the water mass features for the five sub-regions.

(1) The most important atmospheric forcing is the strong winter monsoon (north to northeast) and weak summer monsoon (southeast). The surface air temperature has a nearly latitudinal gradient with a south-to-north difference of 18°C in February and 3°C in August. The surface relative humidity is generally higher in the summer season, mainly as a consequence of the southeast summer monsoon bringing moist air from the tropics. A relative humidity minimum (maximum) is present in all seasons near Kyusyu Island (Chinese coast), which may lead to maximum (minimum) evaporation there.

(2) The air-sea heat budget at the surface is dominated by the incoming solar radiation balanced by latent and longwave heat energy loss. It was found that the Yellow Sea has an overall long term heat gain of 15 W m^{-2} (caused by low latent heat flux), and the rest of the area has an overall heat loss of around 30 W m^{-2} in the East China Sea and Cheju bifurcation zone, and around 65 W m^{-2} in the Kuroshio and Taiwan Warm Current regions. The sensible heat flux is nearly zero in summer, which implies that the SST is close to the SAT. The monthly variation of net surface heat flux is nearly sinusoidal and quite similar among the five sub-areas. Q_{net} peaks in June in the Yellow Sea and in July in the rest of sub-areas.

(3) The air-sea fresh water budget exhibits a distinct winter fresh water loss and summer fresh water gain pattern. The whole area experiences an overall fresh water loss (1.8-4 cm/month) at the surface.

(4) The East China and Yellow Seas do not follow the usual atmospheric seasons. We divide the four seasons based on the relative heat storage, namely, winter (January-April), spring (May-June), summer (July-November), and autumn (December).

(5) We classify the water masses of the East China and Yellow Seas using climatological averages. The entire water column of the East China Sea shelf water and the Yellow Sea (including the Cheju bifurcation zone) undergoes a seasonal thermal cycle with maximum values of temperature during summer, and maximum mixed layer depths during winter. However, only the surface waters of the Taiwan Warm Current (upper 60 m) and the Kuroshio region (upper 80 m) exhibit a seasonal thermal cycle. Below these depths, there is no seasonal variation evident.

(6) The salt balance of the surface layer is clearly affected by the surface fresh water flux and river run-off. In the East China Sea shelf region, the surface freshness (low salinity) is in phase with the surface fresh water flux (P - E) and out of phase with the Yangtze River water discharge. The lowest surface salinity (spring) does not occur at the same time as the maximum Yangtze River discharge (July). In the Yellow Sea, however, the surface freshness is out of phase with the surface fresh water flux (P - E) and in phase with the Yangtze River water discharge. Two different relations between surface salinity and Yangtze River run-off, out of phase in the East China Sea shelf and in phase in the Yellow Sea, may confirm an earlier study by Beardsley et al. (1985) that the summer fresh water discharge from the Yangtze River forms a relatively shallow, low salinity plume-like structure extending offshore on average towards the northeast.

(7) The thermohaline structure of the East China Sea and Yellow Sea experiences a strong interannual variation. Among five sub-regions, the shallow areas (ECS, YS, CB, TWC) experience a larger interannual variation than the deep area (KC). During 1983-1984, a strong cooling and freshening period was found, especially in the Yellow Sea (-8.4°C temperature anomaly in 1984).

LIST OF REFERENCES

Artegiani, A., D. Bregant, E. Paschini, N. Pinardi, F. Raicich, and A. Russo, The Adriatic Sea General Circulation. Part I: Air-sea Interactions and Water Mass Structure, *J. Phys. Oceanogr.*, 27, 1,492-1,514, 1997.

Beardsley, R. C., R. Limeburner, H. Yu, and G. A. Cannon, Discharge of the Changjiang (Yangtze River) into the East China Sea, *Continental Shelf Res.*, 4, 57-76, 1985.

Chen, C.S., R.C. Beardsley, R. Limeburner, and K. Kim, Comparison of Winter and Summer Hydrographic Observations in the Yellow and East China Seas and Adjacent Kuroshio during 1986, *Continental Shelf Res.*, 14, 909-929, 1994.

Chu, P. C., S. K. Wells, S. D. Haeger, C. Szczechowski, and M. Carron, Temporal and Spatial Scales of the Yellow Sea Thermal Variability, *J. Geophys. Res.*, 102, 5,655-5,667, 1997a.

Chu, P. C., C. R. Fralick Jr., S. D. Haeger, and M. J. Carron, A Parametric Model for the Yellow Sea Thermal Variability, *J. Geophys. Res.*, 102, 10,499-10,507, 1997b.

Chu, P. C., H. C. Tseng, C. P. Chang, and J. M. Chen, South China Sea Warm Pool Detected in Spring from the Navy's Master Oceanographic Observational Data Set (MOODS), *J. Geophys. Res.*, 102, 15,761-15,771, 1997c.

Fofonoff, N. P., and R. C. Millard Jr., Algorithms for Computation of Fundamental Properties of Seawater, *UNESCO Tech. Papers in Marine Science*, 44, 53, 1983.

Guan, B. X., Patterns and Structures of the Currents in Bohai, Huanghai and East China Seas, *Oceanology of China Seas.*, vol.1, 17-26, Kluwer, Boston, 1994.

Hecht, A., Z. Rosentroub, and J. Bishop, Temporal and Spatial Variations of Heat Storage in the Eastern Mediterranean, *Isr. J. Earth Sci.*, 34, 51-64,1985.

Hotelling, H., Analysis of a Complex of Statistical Variables into Principal Components, *J. Educ. Psychol.*, 24, 417-441, 498-520, 1933.

Langhill, R. H., Forecasting guide for the Republic of Korea, Det. 18, 20th Weather Squadron, 1st Weather Wing, USAF, 1976.

Li, H. and Y. Yuan, On the Formation and Maintenance Mechanisms of the Cold Water Mass of the Yellow Sea, *Chinese J. Oceanol. Limonol.*, 10 (2), 97-106, 1992.

Lie, H. J., Wintertime Temperature-Salinity Characteristics in the Southeastern Hwanghae (Yellow Sea), *J. Oceanogr. Soc. Japan*, 41, 291-298, 1985.

Lie, H. J., Summertime Hydrographic Features in the Southeastern Hwanghae (Yellow Sea), *Prog. Oceanogr.*, 17, 229-242, 1987.

Liu, S., X. Shen, Y. Wang, and S. Han, Preliminary Analysis of Distribution and Variation of Perennial Monthly Mean Water Masses in the Bohai Sea, the Huanghai Sea and the East China Sea, *Acta Oceanologica Sinica,* 11, 483-498, 1992.

Levitus, S., and T. P. Boyer, World Ocean Atlas 1994 volume 4: Temperature, *NOAA Atlas NESDIS 4,* U.S. Department of Commerce, Washington D.C., 1-117, 1994.

Mao H. L., and B. Guan, A Note on the Circulation of the East China Sea, *Chinese J. Oceanol. Limonol.*, 1, 5-16, 1982.

Niino, H., and K. O. Emery, Sediments of Shallow Portions of East China Sea and South China Sea, *Geolog. Soc. Amer. Bull.,* 72, 731-762, 1961.

Richman, M. B., Rotation of Principal Components, *J. Climatol.,* 6, 193-235, 1986.

Su, Y. S., and X. C. Weng, Water Masses in China Seas, *Oceanology of China Seas*, vol. 1, Kluwer, Boston, 3-16, 1994.

Tomczak, M., and J. S. Godfrey, *Regional Oceanography: An Introduction,* 179-189, CSIRO Division of Oceanography, Tasmania, Australia, 1994.

Van Loon, H. , Climates of the Oceans, *World Survey of Climatology*, 15, 453-458, Elsevier, New York, 1984.

Watts, I. E. M., Climates of China and Korea, *World Survey of Climatology*, 8, 1-117, Elsevier, New York, 1969.

Weare, B. C., A.R. Navato, and R. E. Newell, Empirical Orthogonal Analysis of Pacific Sea Surface Temperature, *J. Phys. Oceanogr.*, 6, 671-678, 1976.

Yanagi, T. and S. Takahashi, Seasonal Variation of Circulations in the East China Sea and the Yellow Sea, *J. Oceanogr.*, 49, 503-520, 1993.

INITIAL DISTRIBUTION LIST

No. Copies

1. Defense Technical Information Center 2
   8725 John J. Kingman Rd., Ste 0944
   Ft. Belvoir, VA 33060-6218

2. Dudley Knox Library 2
   Naval Postgraduate School
   411 Dyer Rd.
   Monterey, CA 93943-5101

3. Superintendent 1
   Attn: Chairman, Department of Oceanography (Code OC/BF)
   Naval Postgraduate School
   Monterey, CA 93943-5002

4. Superintendent 1
   Attn: Chairman, Department of Meteorology (Code MR/WX)
   Naval Postgraduate School
   Monterey, CA 93943-5002

5. Superintendent 1
   Attn: Professor Peter C. Chu (Code OC/CU)
   Naval Postgraduate School
   Monterey, CA 93943-5002

6. Superintendent 1
   Naval Research Laboratory
   7 Grace Hopper Avenue Stop 2
   Monterey, CA 93943-5502

7. Chairman 1
   Oceanography Department
   U.S. Naval Academy
   Annapolis, MD 21402

8. Dr. Manuel Fiadeiro 1
   Office of Naval Research (Code 322OM)
   800N. Quincy Street
   Arlington, VA 22217

9. Library 1
Scripps Institution of Oceanography
P.O. Box 2367
La Jolla, Ca 92037

10. Dr. Martha Head 1
Naval Oceanographic Office (Code N53)
Stennis Space Center, MS 39522

11. Dr. Mike Carron 1
Naval Oceanographic Office (Code N3T)
Stennis Space Center, MS 39522

12. NOAA Library 1
7600 Sand Point Way NE
Building 3
Seattle, WA 98115

13. Lieutenant Commander Akira Kuninaka 1
4-13-1-152 Uragou, Yokosuka-city
Kanagawa, Japan 237-0062